Contents lists available at ScienceDirect

Arabian Journal of Chemistry

journal homepage: www.ksu.edu.sa

Original article

Exploring the efficacy of Congo Red dye as a corrosion inhibitor for aluminum in HCl solution: An interdisciplinary study with RSM modeling and theoretical simulations

Ayoub Chahid [a,b], Mohammed Chafi [b], Mohamed Essahli [a], Awad A. Alrashdi [c,*], Hassane Lgaz [d,*]

[a] Laboratory of Applied Chemistry and Environment (CAE), Faculty of Sciences and Techniques, University Hassan 1, Settat, Morocco
[b] Laboratory of Environment, Processes and Engineering (LEPE), Higher School of Technology (EST), University Hassan II, Casablanca, Morocco
[c] Chemistry Department, Umm Al-Qura University, Al-Qunfudah University College, Al Qunfudah 21962, 11, Saudi Arabia
[d] Innovative Durable Building and Infrastructure Research Center, Center for Creative Convergence Education, Hanyang University ERICA, 55 Hanyangdaehak-ro, Sangrok-gu, Gyeonggi-do, Ansan-si 15588, South Korea

ARTICLE INFO

Keywords:
Corrosion inhibition
Acid solution
Congo Red dye
Response surface methodology
Density functional theory
Molecular dynamics

ABSTRACT

This study investigates Congo Red Textile Dye (CRD) as a corrosion inhibitor for aluminum in a 1.0 mol/L hydrochloric acid solution. Utilizing a comprehensive suite of analytical techniques, including gravimetric analysis, scanning electron microscopy (SEM), ultraviolet–visible spectrophotometry (UV–Vis), Electrochemical Impedance Spectroscopy (EIS), and Potentiodynamic Polarization curves (PDP), we assessed CRD's adsorption mechanism and its corrosion inhibition effectiveness. Significant corrosion mitigation was observed, with the efficiency of inhibition EI (%) increasing alongside CRD concentration, achieving a maximum efficiency of 87.5 %. This enhancement in EI (%) decreases with rising temperatures, assessed across a range from 298 to 323 K. Response surface methodology (RSM) and central composite design (CCD) were employed for accurate corrosion rates (V_{corr}) and EI (%) prediction. Additionally, theoretical analysis was performed using global and local reactivity descriptors along with molecular dynamics (MD) simulations. Theoretical results confirmed the widespread presence of nucleophilic and electrophilic sites, along with a strong affinity for the Al surface, suggesting CRD's potential for enhancing corrosion resistance. This study proposes a potential pathway for the valorization of Congo Red dye, utilizing concentrations within non-toxic thresholds, thereby aligning with environmental safety and industrial application considerations.

1. Introduction

Great technological and economic importance has been given to the corrosion inhibition of aluminum (Al) and its derived alloys, owing to the wide range of their industrial applications. These metals and alloys exhibit high resistance to corrosion in various environments, particularly in aggressive media, which makes them suitable for diverse industrial uses. Generally, in aqueous solutions, aluminum shows passive behavior, increasing its corrosion susceptibility. The adhesive passivated oxide film on the metal surface is amphoteric, so the metal readily dissolves in acidic (Zhao et al., 2020; Wang et al., 2022; Quebbou et al., 2021) or saline solutions (El Mazyani et al., 2021).The prevention of aluminum dissolution is crucial for industries such as chemical, engineering, and pharmaceutical, among others. To address corrosion, various methods have been employed including anodic and cathodic protection, hot-dip galvanizing, coatings, electroplating, environmental modification, inhibitors, lubrication, and painting. Corrosion inhibitors are particularly advantageous as they are simple to apply, cost-effective, and do not require any specialized equipment (Melian et al., 2023; Souza et al., 2023; Assad and Kumar, 2021). These compounds, characterized by polar functional groups and heteroatoms such as oxygen, sulfur, nitrogen, or phosphorus, adhere to the metal surface through electrostatic or chemical bonds, effectively preventing corrosion (Tezcan et al., 2018; Zeinali Nikoo et al., 2020). Organic dyes, especially those with heterocyclic structures, are emerging as potent corrosion inhibitors. Their effectiveness is attributed to a balance of hydrophilicity, hydrophobicity, and conjugation, enhanced by polar functional groups, nonbonding electrons, and multiple bonds in aromatic rings and side chains (El-Katori et al., 2022; Ganjoo et al., 2022b). Azo dyes, constituting over 60 % of all dyes used, are notably effective in metal corrosion inhibition

* Corresponding authors.
E-mail addresses: aarashdi@uqu.edu.sa (A.A. Alrashdi), hlgaz@hanyang.ac.kr (H. Lgaz).

https://doi.org/10.1016/j.arabjc.2024.105810
Received 1 December 2023; Accepted 23 April 2024
Available online 26 April 2024

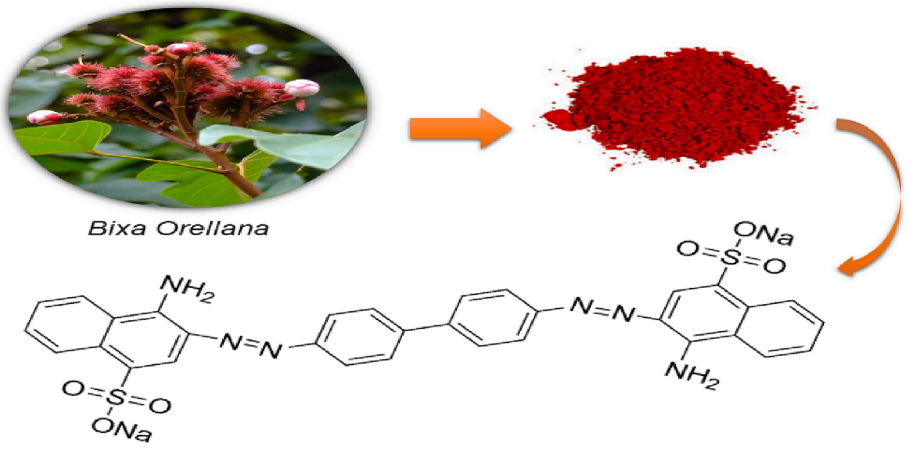

Fig. 1. Molecular structure of the Congo Red Dye (CRD).

and are extensively utilized in various commercial applications (Abdallah et al., 2014; Madkour et al., 2016; Paşka et al., 2014). Known for their excellent donor properties, these dyes play a significant role in coordination chemistry (Al-Gaber et al., 2023), Consequently, the formation of an adsorption coating on metal surfaces, which protects against corrosive attacks, can be achieved through covalent bonding (chemisorption) and/or electrostatic interaction (physisorption) (Fouda et al., 2022). he chemisorption behavior of these dyes, involving nonbonding electrons and π-electrons, plays a significant role in mitigating corrosion through interactions with metallic surfaces. These characteristics enable them to efficiently bind to metal surfaces in aqueous electrolytes, acting as polydentate and chelating ligands (El-Katori et al., 2022; Ganjoo et al., 2022b).

In addition to their functional efficacy, the use of these dyes at low concentrations is particularly advantageous due to their non-toxic nature, making them safer for both industrial applications and the environment (El-Katori et al., 2022; Ganjoo et al., 2022b; Oladoye et al., 2022). The shift towards eco-friendly options, such as natural and semi-synthetic dyes, underscores this advantage. These dyes, soluble in both water and organic solvents, offer an environmentally responsible approach to corrosion inhibition, aligning with sustainability goals without compromising on performance. Their non-toxicity at low concentrations presents a dual benefit of effective corrosion prevention and adherence to environmental safety standards. Congo Red dye (CRD) is an important azo dye used in various industries such as textiles, plastics, rubber, paper, and printing (Oladoye et al., 2022).

Molecular dynamics (MD) simulations and density functional theory (DFT) calculations are frequently utilized to elucidate the mechanisms of corrosion inhibition (Obot and Gasem, 2014; Zeng et al., 2013). MD simulations offer a microscopic view, facilitating an intuitive understanding of system evolution under specific conditions, while DFT provides a quantum analysis of electron structures (Chen et al., 2021).

This work aims to examine the inhibitory effect of CRD on aluminum corrosion in a 1.0 mol/L HCl solution under different experimental conditions. The purposes are firstly, to determine the thermodynamic parameters associated with the adsorption process, shedding light on the mechanism of adsorption inhibition on the aluminum surface; and secondly, to optimize the obtained results in HCl solutions through experimental design (DOE) and the specific methodology of Response Surface Methodology (RSM) using the Central Composite Design (CCD). Finally, we aim to conduct density functional calculation studies to determine the global and local chemical reactivity descriptors. Additionally, molecular dynamics simulation was used to estimate the adsorption energy and structural configuration of the dye on the aluminum surface.

2. Materials and methods

2.1. Selected inhibitor and solution

The chosen corrosion inhibitor is an organic dye called Congo Red (CRD) frequently used in the coloring of textiles, which is part of the poly azo category, its molar mass is 696.663 g mol^{-1}. Fig. 1 shows its molecular structure. This work intends to suggest a potential pathway for the valorization of Congo Red dye, utilizing concentrations that fall within non-toxic thresholds. The corrosive solution used is 1.0 mol/L HCl, which was prepared by diluting 37 % Hydrochloric acid in distilled water. Test solutions were freshly prepared before each experiment by adding the inhibitor directly to the corrosive solution at various concentrations of CRCs. These experiments were repeated three times to ensure reproducibility.

2.2. Gravimetric measurements

Gravimetric tests were conducted after verifying the desired electrolyte temperature using a thermostat (Selecta Frigitherm) with a 0.1 °C margin of error. The selected electrolyte volume was 80 mL. The samples had a rectangular shape with dimensions of 2.0 cm × 1.0 cm × 0.1 cm, and each coupon has a hole with a diameter of 0.2 cm drilled into it. They are then attached with a thread of cloth so that they can hang freely in the solutions to be examined. Before taking measurements, they undergo mechanical polishing with different types of sandpaper (P400 - P1200) until achieving a mirror-like finish. Prior to immersing the samples in the test solution, the dimensions of each coupon are checked. Then, they are washed with distilled water and dried. The cleaned aluminum coupons were weighted before and after the immersion. The *EI(%)* values of CRD are deduced using Eq. (1):

$$EI(\%) = \frac{W_0 - W}{W_0} \times 100 \quad (1)$$

where W and W_0 represent the sample mass in the presence and absence of the CRD inhibitor, respectively. The corrosion rate (in $g{\cdot}cm^{-2}{\cdot}h^{-1}$) is determined by calculating the variation between the initial weight and the final weight of each coupon after each immersion step, as it indicated in Eq. (2):

$$V_{corr} = \frac{W_0 - W}{At} \times 100 \quad (2)$$

where 't' is the exposure time in hours and 'A' is the area of the sample in (cm^2).

Table 1
Chemical composition of the aluminum alloy identified by fluorescence X.

Compound	Concentration	Unit	Compound	Concentration	Unit
Al	91.371	%	**Ni**	27.7	ppm
Si	0.268	%	**Cu**	10.6	ppm
Fe	0.276	%	**Zn**	29.9	ppm
S	303.4	ppm	**Ga**	85.4	ppm
Cl	613.6	ppm	**Zr**	15.3	ppm
K	224.8	ppm	**Ag**	243.6	ppm
Ca	135.8	ppm	**Eu**	8.2	ppm
Ti	175.8	ppm	**Yb**	0.0	ppm
V	85.4	ppm	**Re**	0.9	ppm
Cr	10.6	ppm	**Tl**	0.0	ppm
Mn	42.5	ppm	**Pb**	6.0	ppm

2.3. Electrochemical measurements (OCP, EIS, and PDP)

The inhibitory effectiveness of the examined inhibitor against aluminum corrosion was evaluated utilizing a PGZ301 electrochemical workstation model. The assessment involved both Potentiodynamic Polarization (PDP) and Electrochemical Impedance Spectroscopy (EIS) measurements in a 1.0 mol/L solution, under different CRD concentration conditions. A conventional three-electrode cell was employed, comprising an aluminum specimen as the working electrode, a saturated calomel electrode (SCE) as the reference electrode, and a platinum grid as the counter electrode. Prior to conducting measurements, the working electrode was submerged in a 1.0 mol/L solution, both without and with various CRD concentrations, and allowed to equilibrate for 30 min at the open circuit potential (OCP). The PDP plots were generated using a scan rate of 0.5 $mV{\cdot}S^{-1}$ within the standard potential range determined by adding ±200 mV to the OCP. EIS spectra were collected at OCP across a frequency range from 100 kHz to 10 mHz with an amplitude of 10 mV. Three replicas of the trials were performed, and the average values were regarded. The inhibitory efficacy η_p by the PDP Technique and surface coverage θ on the working electrode surface were assessed as follows (Kellal et al., 2023a,2023b):

$$\eta_p = \frac{i^0_{corr} - i^{inh}_{corr}}{i^0_{corr}} \times 100 \quad (3)$$

$$\theta = \frac{i^0_{corr} - i^{inh}_{corr}}{i^0_{corr}} \quad (4)$$

where i^0_{corr} ($mA{\cdot}cm^{-2}$) and i^{inh}_{corr} are the corrosion current densities of uninhibited and inhibited electrolyte solutions, respectively.

$$\eta_{EIS} = \frac{R_p - R^0_P}{R_p} \times 100 \quad (5)$$

where R^0_P and R_p are the polarization resistance in the absence and presence of the CRD compound in the HCl medium. η_{EIS} represents the corrosion inhibition efficiency, assessed through Electrochemical Impedance Spectroscopy analysis.

2.4. X-ray fluorescence and scanning electron microscope

A sample cut in the form of a circular coupon of the same dimensions as that of the sample holder dedicated to X-ray fluorescence spectrometry. The obtained results by x-ray fluorescence analysis are shown in Table 1.

The aluminum (Al) surface was characterized by scanning electron microscopy (SEM) before and after immersion in 1.0 mol/L HCl for 4 h at 25 °C, both in the absence and presence of an inhibitor. After completing the immersion test, the Al surface was washed with distilled water, dried, and subsequently inspected using SEM.

2.5. UV–visible spectrophotometric study

The electrolytes used for weight loss testing are evaluated using a UVmini-1240 Spectrophotometer. This evaluation aims to confirm the formation of the Al-inhibitor complex that may occur when aluminum is immersed in a hydrochloric acid electrolyte containing inhibitor molecules.

2.6. Response surface methodology

The methodology incorporated a range of immersion times for corrosion tests, spanning 1, 2, 3, and 4 h, to examine the temporal effects on corrosion inhibition. The study also varied the concentrations of the inhibitor, Congo Red, testing levels at 200, 400, 600, 800, 1000, 1200, and 1400 ppm to determine the optimal inhibitory concentration. To assess the impact of temperature, experiments were conducted at 25, 30, 40, 50, and 60 °C. The collected data in the hydrochloric acid medium were then optimized using Response Surface Methodology (RSM) based on the Central Composite Design (CCD). This optimization process utilized the response data from the corrosion experiments to enhance the model, allowing for the determination of optimal data points among the varied factors. The resulting model provides a predictive framework for understanding response variables under specified environmental conditions.

2.7. Computational details

2.7.1. Density functional theory details

Quantum chemical simulations were conducted using the DMol3 code based on Density Functional Theory (DFT) implemented in Materials Studio package. Calculations of parameters were conducted using the B3LYP functional with a DNP basis set (basis file 4.4), alongside Fermi smearing of 0.005 Ha and a global cutoff of 3.7 Å, we enforced an SCF convergence tolerance of 1×10^{-6}. To simulate the solvent effect of water (with a dielectric constant $\varepsilon = 78.54$), we employed the Conductor-like Screening Model (COSMO) (Klamt, 2018). This approach to understand how molecular structures and electronic properties influence the efficacy of inhibitor adsorption on the metal surface (Nyijime et al., 2023). The (DNP) basis set, incorporating d and p polarization. Prior studies have demonstrated that the DNP basis set offers comparable quality to the 6-31G Gaussian basis set and superior accuracy compared to Gaussian basis sets of similar size (Migahed et al., 2016; Feng et al., 2018). After optimizing the geometric structure, the following quantum parameters, including the energy of the lowest unoccupied molecular orbital (E_{LUMO}) and the energy of the highest occupied molecular orbital (E_{HOMO}), energy gap (ΔE), dipole moment (μ), electronegativity (χ), ionization potential (I), electron affinity (A), hardness (η), softness (σ), and the extent of electron transfer from the inhibitor molecule to the metal surface (ΔN) Ionization energy (IP), and The $\Delta E_{back\text{-}donation}$ energy, are determined as chemical reactivity descriptors using the following equations (Dagdag et al., 2020):

$$I: \text{ionization potential} = -E_{HOMO} \quad (6)$$

$$A: \text{electron affinity} = -E_{LUMO} \quad (7)$$

$$\Delta E_{gap}: \text{the energy gap (eV)} = E_{LUMO} - E_{HOMO} \quad (8)$$

$$\chi: \text{absolute electronegativity} = \frac{I + A}{2} \quad (9)$$

$$\eta: \text{Global hardness} = \frac{I - A}{2} \quad (10)$$

$$S: \text{Global softness} = \frac{1}{\eta} \quad (11)$$

$$\omega:\ \text{Global electrophilicity index} = \frac{\mu 2}{2\eta} \tag{12}$$

where Electronic chemical potential = −Electronegativity; μ = −X (Al, 2020).

$$\Delta E\ \text{Back} - \text{donation Energy}:\ \text{the back donation} = -\frac{\eta}{4} \tag{13}$$

The $\Delta E_{\text{back-donation}}$ quantifies the energy associated with metal atoms donating electrons to inhibitor molecules on aluminum surfaces. It characterizes the propensity for electron transfer, crucial in understanding inhibitor-surface interactions (Belal et al., 2023).

(ΔN): the fraction of electron transferred was determined using Eq. (14) (Guo et al., 2021):

$$\Delta N = \frac{\chi_{Al} - \chi_{inh}}{2(\eta_{Al} + \eta_{inh})} \tag{14}$$

χ_{inh} and η_{inh} indicate the absolute electronegativity and hardness of the inhibitor molecule, while χ_{Al} and η_{Al} represent those of aluminum, respectively.

A theoretical value for the electronegativity (χ_{Al} = 5.60 eV) of aluminum (Al) with a global hardness of η_{Al} = 0 eV was used (Iorhuna et al., 2023).

The local reactivity of the inhibitor compound was investigated by examining the Fukui indices (Boukerche et al., 2023). At a constant external potential $v(\vec{r})$, the Fukui function (f_k) is defined as the initial derivative of the electronic density $\rho(\vec{r})$ with respect to the number of electrons (N) (Chadili et al., 2021a).

$$f_k = \left(\frac{\partial \rho(\vec{r})}{\partial N}\right) v(\vec{r}) \tag{15}$$

The electron charge distribution on the CRD molecules was determined, these findings can be used to calculate Fukui indices (f_k^- and f_k^+) for local electrophilic and nucleophilic or radical attacks. To calculate the Fukui functions, the following finite difference approximations were used (Corrosion Inhibitive Potentials of some 2H-1-benzopyran-2-one Derivatives- DFT Calculations, 2021):

$$f_k^+ = q_{k(N+1)} - q_{k(N)} \quad (\textit{for a nucleophilic attack}) \tag{16}$$

$$f_k^- = q_{k(N)} - q_{k(N-1)} \quad (\textit{for a electrophilic attack}) \tag{17}$$

$$f_k^0 = \left(\frac{\partial \rho(\vec{r})}{\partial N}\right) \tag{18}$$

$$f_k^0 = \frac{q_{k\,(N+1)} - q_{k(N-1)}}{2} \quad (\textit{for radical attack}) \tag{19}$$

where q_k represents the global charge of the k atom, i.e., the electronic density at a specific point (r) in space around the molecule in question. The $q_{k(N)}$, $q_{k(N+1)}$ and $q_{k(N-1)}$ are defined as the charge of the neutral, cationic and anionic species, respectively.

2.7.2. Molecular dynamic (MD) simulations

Molecular Dynamics (MD) simulations were employed to ascertain the most effective adsorption configuration of the Congo Red Dye (CRD) on the aluminum surface, utilizing the Forcite module in Materials Studio software. The procedure began with extracting a unit cell of pure aluminum (Al) from the software's database, to create the Al(1 1 0) surface. The Al(1 1 0) surface was selected for molecular dynamics simulations of corrosion inhibition in HCl solution due to its structural and energetic characteristics, which influence oxygen adsorption rates and oxide growth dynamics. This surface orientation allows for a detailed examination of the inhibitor interactions due to its high surface energy and reactivity, providing valuable insights into the inhibition mechanisms at an atomic level (Kim and Choi, 2021; Lim and Zhong, 2009). The unit cell was then expanded fivefold in both x and y directions, forming a super-cell measuring 48.594 Å × 34.361 Å × 35.748 Å. To mitigate inter-supercell interactions attributable to periodic boundary conditions, a vacuum layer of 25 Å was established (Chadili et al., 2021b). The simulation setup included a solvent layer, composed of the optimized dye molecule, 500 water molecules, along with 5 chloride ions (Cl^-) and 5 hydronium ions (H_3O^+). The smart algorithm was applied to fine-tune the geometry of the initial adsorption system (Mehmeti and Podvorica, 2018). The computational model addressed electrostatic interactions via the Ewald summation method and accounted for Van der Waals forces at an atom-based level, incorporating a cutoff distance of 15.5 Å, a spline width of 1 Å, and a buffer distance of 0.5 Å. The MD simulations operated within the NVT ensemble, which conserves particles, volume, and temperature, ensuring an accurate portrayal of thermal fluctuations crucial for understanding corrosion. Its maintenance of constant temperature closely mirrors experimental conditions (Haris et al., 2021). Simulations spanned a duration of 300 picoseconds with a time step of 1.0 fs, employing the COMPASS force field (Umar and Uzairu, 2019). Temperature control of the simulated system, set at 298 K, was achieved using the Andersen thermostat. To quantify the interaction dynamics, two critical energy metrics were calculated: the interaction energy ($E_{interaction}$) and the binding energy ($E_{Binding}$). $E_{interaction}$ was derived using the formula (Daoudi et al., 2022; Ganjoo et al., 2022a):

$$E_{interaction} = E_{total} - (E_{surface+solution} + E_{inhibitor}),$$

where E_{total} represents the total energy of the simulation system, $E_{inhibitor}$ denotes the energy of the free inhibitor molecule, and $E_{surface+solution}$ signifies the energy of the aluminum surface combined with water molecules, chloride, and hydronium ions. The binding energy was determined as the negative value of the interaction energy, as defined by the equation: $E_{binding} = -E_{interaction}$.

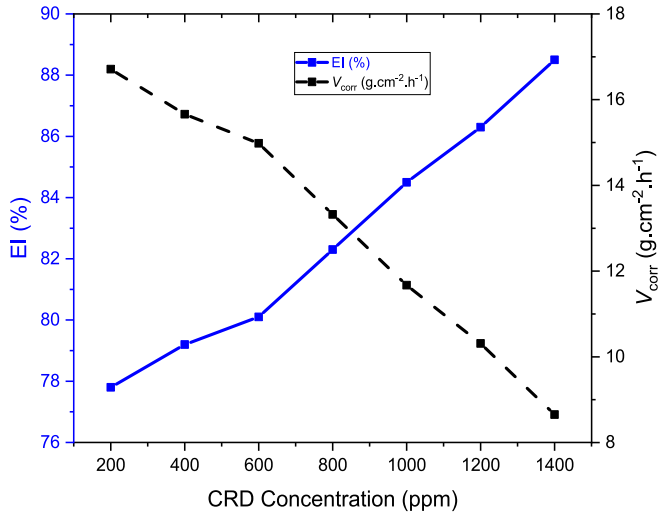

Fig. 2. Corrosion rates (V_{corr}) and inhibition efficiencies (EI%) for aluminum in 1 M HCl with different concentrations of CRD at 298 K during a 2-hour immersion period..

3. Results and discussions

3.1. Inhibitory effect of Congo Red

The weight loss method, an integral technique in the field of corrosion inhibition studies, was employed to evaluate the corrosion rate (V_{corr}) of aluminum samples. This method involves measuring the weight loss of aluminum samples when immersed in a 1.0 mol/L HCl solution, both in the absence and presence of various concentrations of

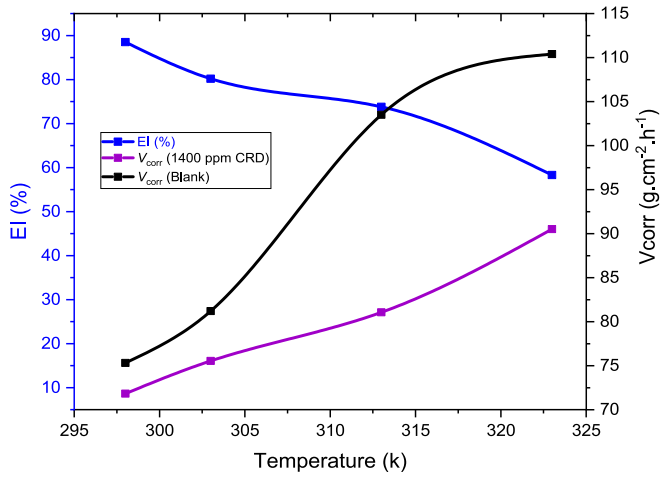

Fig. 3. Corrosion rates (V_{corr}) and inhibition efficiencies (EI%) for aluminum in 1.0 mol/L HCl at different temperatures obtained by the gravimetric method.

Congo Red Dye (CRD), as depicted in Figs. 2 and 3. The data gathered from this approach are instrumental in understanding the dynamics of corrosion processes and provide critical insights into the effectiveness of CRD. The results indicate a notable improvement in the corrosion rate (V_{corr}) of the aluminum samples. It appears that as the concentration of CRD increases, the metal corrosion rate steadily decreases, and its protective efficiency increases. Initially, the dissolution of Al in the corrosive solution is slow and increases with time. This can be ascribed to a pre-immersed Al_2O_3 film persistent on the metal surface (Belafhaili et al., 2023). The non-linearity and non-uniformity of the plots obtained in the inhibited and uninhibited solutions suggest that the Al corrosion process is heterogeneous with several stages (Ating et al., 2010). Acid solutions attack the free aluminum surface and therefore, deterioration of the metal structure.

In the acidic environment, Al undergoes a series of successive electrochemical reactions (Raghavendra and Ishwara Bhat, 2018):

$$Al_2O_3 + 3H_2O \rightarrow 2Al(OH)_3$$

$$Al(OH)_3 + H^+ \rightarrow Al(OH)_2^+ + H_2O$$

$$Al(OH)_2^+ + 2H^+ \rightarrow Al^{3+} + 2H_2O$$

Overall reaction:

$$Al_2O_3 + 6H^+ \rightarrow 2Al^{3+} + 3H_2O$$

Al^{3+} exists as $Al[(H_2O)_6]^{3+}$ in acid solution

The corrosion of aluminum in hydrochloric acid solutions initiates with the adsorption of chloride ions (Cl^-) onto the aluminum surface's active sites, a critical step that undermines the integrity of the aluminum oxide layer, particularly in acidic conditions, rendering it susceptible to dissolution (Anh et al., 2020; Padash et al., 2018). The destabilization of the protective oxide layer, driven by its inherent instability under such conditions, is marked by the development of a positive surface charge, which inherently attracts Cl- ions, further exacerbating the corrosion process (El-Sayed et al., 2023), this phenomenon not only facilitates the initial adsorption of Cl^- ions but also results in the differential reactivity across the aluminum surface, where unaffected regions are primed to serve as cathodic sites (Padash et al., 2020). These cathodic areas are crucial, supporting reduction reactions that, together with anodic dissolution, significantly increase the corrosion rate of aluminum. This intricate interplay of electrochemical reactions, dictated by the spatial distribution of anodic and cathodic sites, is further complicated by the formation of oxide-Cl- complexes. These complexes, which arise from the interaction between Cl- ions and the aluminum oxide layer, prevent passive film formation and accelerate anodic dissolution (Yoo et al., 2016). Together, these processes underscore the multifaceted nature of aluminum corrosion in acidic environments, offering profound insights into the mechanisms through which Cl- ions destabilize the aluminum oxide layer, thereby impeding passive film formation and catalyzing anodic dissolution (Lee and Pyun, 1999).

Table 2
Activation parameters for aluminum in HCl in the absence and the presence of the CRD inhibitor.

C_{inh} (ppm)	E_a (kJ /**mol**)	ΔH_a^0 (kJ/mole)	ΔS_a^0 (J/mol K)
Blank	93.36	90.87	−344.56
1000 ppm	103.26	100.81	−352.21

Table 3
Thermodynamic parameters for the adsorption of the inhibitor for aluminum in HCl at 298 K.

	K_{ads} (L/mol)	Slope	R^2	ΔG_{ads}^0 (KJ/mol)
CRD	0.9057	1.1035	0.9974	−9.73

In HCl, the cathodic reaction is defined by the reduction of H^+. The initial rapid increase in weight loss aligns with the quick dissolution of the amphoteric air-formed oxide layer on the metal. This exposure of the freshly prepared aluminum surface results in the rapid dissolution of the substrate metal (Oki et al., 2013). Moreover, the weight loss of Al is found (Fig. 3) to decrease by the increase of CRD doses. This signifies that CRD reduces the corrosion of Al as a result the dye has an inhibitory effect. CRD forms a protective adsorption film that blocks the surface of the metal, separating it from the corrosive medium is thus the reduction of the Al dissolution (Sanni et al., 2022).

At the metal/solution interface, four categories of adsorption can occur: (1) the interaction of the uncharged electron pair in the molecule with the metal, (2) electrostatic attraction between the charged metal and the charged molecules, (3) the interaction of π electrons with the metal, and (4) a combination of (2) and (3) (Fouda et al., 2015). The inhibitory molecules are adsorbed onto the metal surface either by physisorption or chemisorption. The chemisorbed molecules reduce the metal's inherent reactivity at the adsorption sites, thereby inhibiting the anodic reaction, while the physisorbed molecules inhibit the cathodic reaction by effectively delaying the metal's dissolution (K et al., 2016; Harvey et al., 2018).

Given the dependence of EI(%) on the CRD concentration shown in (Fig. 3), it appears that the inhibitor will act by adsorbing and blocking the active center necessary for the dissolution of aluminum. Namely, the inhibitor reduces the active center for Al dissolution, the adsorption mechanism is made possible by the presence of heteroatoms such as N and O which are considered active adsorption centers. The CRD molecule contains phenyl rings with π electrons, oxygen, nitrogen, and N = N (azo group). The inhibitor could be adsorbed on the surface of Al by the interaction between the pair of electrons of the nitrogen and oxygen atoms or by the π systems of the aromatic rings which are rich in electrons or with the azo group (Boudalia et al., 2023).

3.2. *Effect of CRD concentrations*

The inhibition efficiency (EI%) and corrosion rate V_{corr} of aluminum, determined using the weight loss method in an HCl solution both in the absence and presence of various inhibitor concentrations (ranging from 200 to 1400 ppm), are illustrated in Fig. 2. The results demonstrate an increase in inhibition level with a rise in inhibitor concentration, aligning with the theory of adsorption on a metal surface (Kumar et al., 2004). Fig. 2 shows that the EI% increases rapidly with increasing CRD in the HCl solution. Electrochemical findings from Tables 2 and 3 reinforce the trend observed in weight loss data, affirming the increased

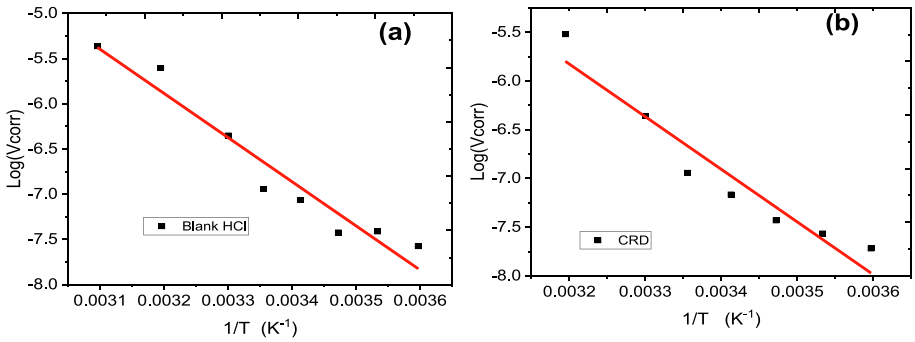

Fig. 4. Arrhenius diagrams of the corrosion rate of aluminum in 1.0 mol/L HCl in the absence (a) and in the presence (b) of 1000 ppm CRD inhibitor.

inhibition efficacy with higher CRD concentrations.

At a concentration of 200 ppm, the inhibition efficiency is 77.8 %, suggesting partial surface coverage. When the concentration increases to 1400 ppm, the efficiency peaks at 88.5 %, indicative of a denser and more uniform protective layer on the aluminum surface. This trend suggests that at higher concentrations, CRD enhances the barrier against corrosion predominantly through physisorption, as evidenced by the increased layering of CRD molecules on the metal. The clear correlation between concentration and inhibition underscores CRD's potential as an effective physisorption-based corrosion inhibitor for aluminum. Furthermore, given aluminum's susceptibility to corrosion, this observation suggests that the predetermined test conditions likely enhanced CRD's affinity for adsorption sites on the aluminum surface. Such enhanced affinity may be a key factor in CRD's observed effectiveness at mitigating corrosion under these specific experimental parameters.

3.3. Temperature effect on the corrosion inhibition action

Temperature plays a significant role in influencing the corrosion rate of metals and the adsorption of inhibitor molecules on electrode surface, especially in aggressive environments (El Mazyani et al., 2021). To understand the impact of temperature on the corrosion rate of aluminum alloys in a 1.0 mol/L HCl solution with an optimal inhibitor concentration, our study focused on a temperature range of 298–323 K. We conducted weight loss measurements (Fig. 3) and employed the PDP and EIS techniques to generate the corresponding results, as presented in Figs. 7 and 8, both in the absence and presence of the inhibitor. The temperature factor significantly increases the corrosion rate in both inhibited and uninhibited solutions, This observation aligns with findings reported by Deepa and Padmalatha (2017). The same behavior has been observed with a few other azo dyes (Fiori-Bimbi et al., 2015; Abboud et al., 2009). This can be attributed to the potential for increased temperatures to induce inhibitor molecule desorption from the metal surface (Chakravarthy et al., 2014; Chakravarthy et al., 2014), resulting in metal dissolution and a decrease in the effectiveness of the tested azo dye inhibitor. Based on the PDP results, it can be observed that a temperature increase from 298 to 323 K led to a decrease in inhibition efficiencies, declining from 86.34 % to 60.99 %. This effect could be attributed to potential CRD structure degradation or a weakening of the adsorption process. It may also suggest a physical nature of the CRD adsorption process, where a temperature rise might lead to the desorption of some physically adsorbed CRD molecules, consequently reducing inhibition efficiency (Faustin et al., 2015; Lin et al., 2021).

The Tafel plots presented in Fig. 7 exhibit similarity in curve shapes in the hydrochloric medium, both in the presence and absence of the inhibitor, across all temperatures. This observation indicates that there is no change in the reaction mechanism and suggests that CRD does not alter the underlying electrochemical processes occurring in the anodic and cathodic regions of the specimen surface; instead, it delays them (Abbout et al., 2021; Abbout et al., 2021). The kinetic parameters obtained through Tafel extrapolation in 1 M HCl are provided in Table 3. The data indicates that as the temperature rises, the inhibition efficiency EI% decreases, and the current density in both uninhibited and inhibited solutions also increase. Corrosion of metals in acidic environments typically involves the release of H_2 gas. The adsorption process of the inhibitor may be influenced by the agitation caused by the accelerated evolution of H_2 at higher temperatures, which could potentially lead to a decrease in the corresponding inhibition efficiency (Halambek et al., 2012). This could be explained also by the spontaneous and irreversible nature of the adsorption processes, which result in the release of heat, and the rise in temperature was found to be unfavorable for adsorption. All these findings confirm that the CRD acts as an effective inhibitor for 1.0 mol/L HCl medium in examined temperature ranges.

3.4. Kinetic activation parameters

The energy of activation (E_a) is calculated by the Arrhenius law in the absence and the presence of the CRD inhibitor (Raviprabha et al., 2023):

$$V_{corr} = Ae^{-E_a/RT} \quad (20)$$

A defined the Arrhenius factor. The fitting straights, according to

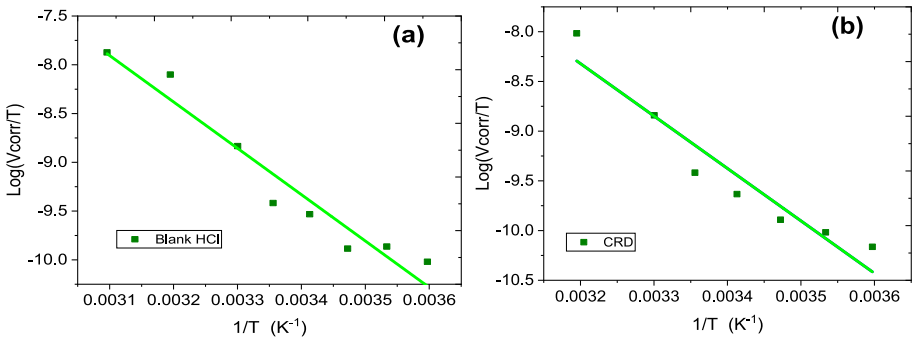

Fig. 5. Variation of log (V_{corr}/T) as a function of 1/T in the absence (a) and the presence (b) of 1000 ppm CRD inhibitor in 1.0 mol/L HCl.

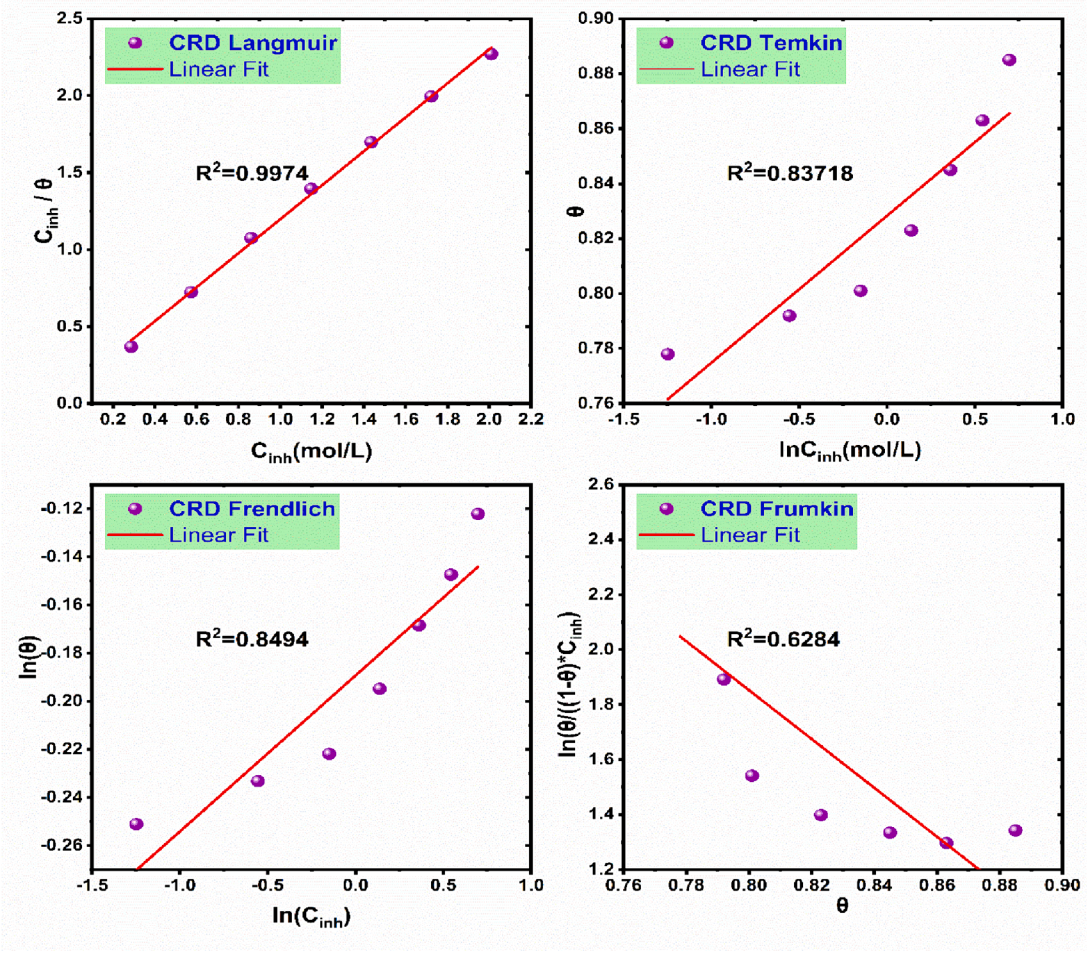

Fig. 6. Plots of the isotherm models for the adsorption of the CRD on the aluminum surface in 1.0 mol/L HCl at 298 K.

Arrhenius law in the absence or presence of CRD inhibitor, are shown in Fig. 4. E_a is estimated from the calculation of the slope ($-E_a/2.3R$) of Arrhenius plots depicted mathematically by Eq. (22):

$$Log(V_{corr}) = Log(A) - \frac{E_a}{2.3RT} \tag{21}$$

Activation enthalpy is obtained by applying the transition state equation (Ikeuba et al., 2023; Bedair et al., n.d):

$$V_{corr} = \frac{RT}{Nh} exp\left(\frac{\Delta S_a^0}{R}\right) exp\left(-\frac{\Delta H_a^0}{RT}\right) \tag{22}$$

were h, ΔS_a^0, ΔH_a^0 and N are respectively the Planck's constant, activation entropy, activation enthalpy, and Avogadro number. The logarithmic form of eq. (22) leads to its linear expression as follows:

$$log\left(\frac{V_{corr}}{T}\right) = Log\left(\frac{R}{Nh}\right) + \frac{\Delta S_a^0}{2.3R} - \frac{\Delta H_a^0}{2.3RT} \tag{23}$$

The activation entropy ΔS_a^0 and the activation enthalpy ΔH_a^0 in the absence or the existence of the CRD inhibitor were anticipated from the linear fit in Fig. 5, which display the changes of $\log(V_{corr}/T)$ vs. $1/T$, where the inclines are expressed by $\left(-\frac{\Delta H_a^0}{2.3RT}\right)$ and the ordinates at the origin by $\left(Log\left(\frac{R}{Nh}\right) + \frac{\Delta S_a^0}{2.3R}\right)$.

The data in Table 2 show that in HCl solutions, the presence of CRD inhibitor increases E_a from 93.36 to 103.26 kJ/mol. The inhibition of the corrosion process is increasingly effective with the rising activation energy (E_a) of the reaction. This increase in E_a is attributed to the formation of an adsorbent layer on the metal surface, which impedes both mass and energy transfer (Al-Amiery et al., 2022). In the presence of CRD, the elevated value of E_a can be interpreted as being due to the decrease of the surface coverage degree by increasing temperature (Lebrini et al., 2013). The suggestion here is that the adsorbed organic matter forms a physical barrier that hinders charge and mass transfer, resulting in a decreased corrosion rate. The increased E_a value observed in the presence of the inhibitor, compared to its absence, can be attributed to physical adsorption (Shivakumar and Mohana, 2013). The positive sign of the enthalpy signifies that the dissolution of aluminum in electrolyte is endothermic process, also the high value of the enthalpy in the presence of the CRD inhibitor discloses to a good inhibition efficacy (Fouda et al., 2016). The increase in activation energy from 93.36 kJ/mol for the blank to 103.26 kJ/mol with 1000 ppm of the CRD inhibitor, and a corresponding increase in the reaction enthalpy change from 90.87 kJ/mol to 100.81 kJ/mol, highlight the endothermic nature of aluminum dissolution in the presence of the inhibitor. These increases suggest that the inhibitor enhances the amount of energy absorbed during the reaction, which is characteristic of an endothermic process where heat is absorbed from the surroundings to facilitate the reaction. Furthermore, the decrease in entropy from −344.56 J/mol·K to −352.21 J/mol·K with the inhibitor implies a more ordered system. In endothermic reactions, such ordering often correlates with the absorption of heat, which stabilizes the inhibitor molecules at the surface, forming more structured and stable complexes. The ordering effect and increased heat absorption induced by the CRD inhibitor suggest its role in stabilizing the aluminum surface, making the dissolution process require more energy and thus, proceed more slowly.The increase in the

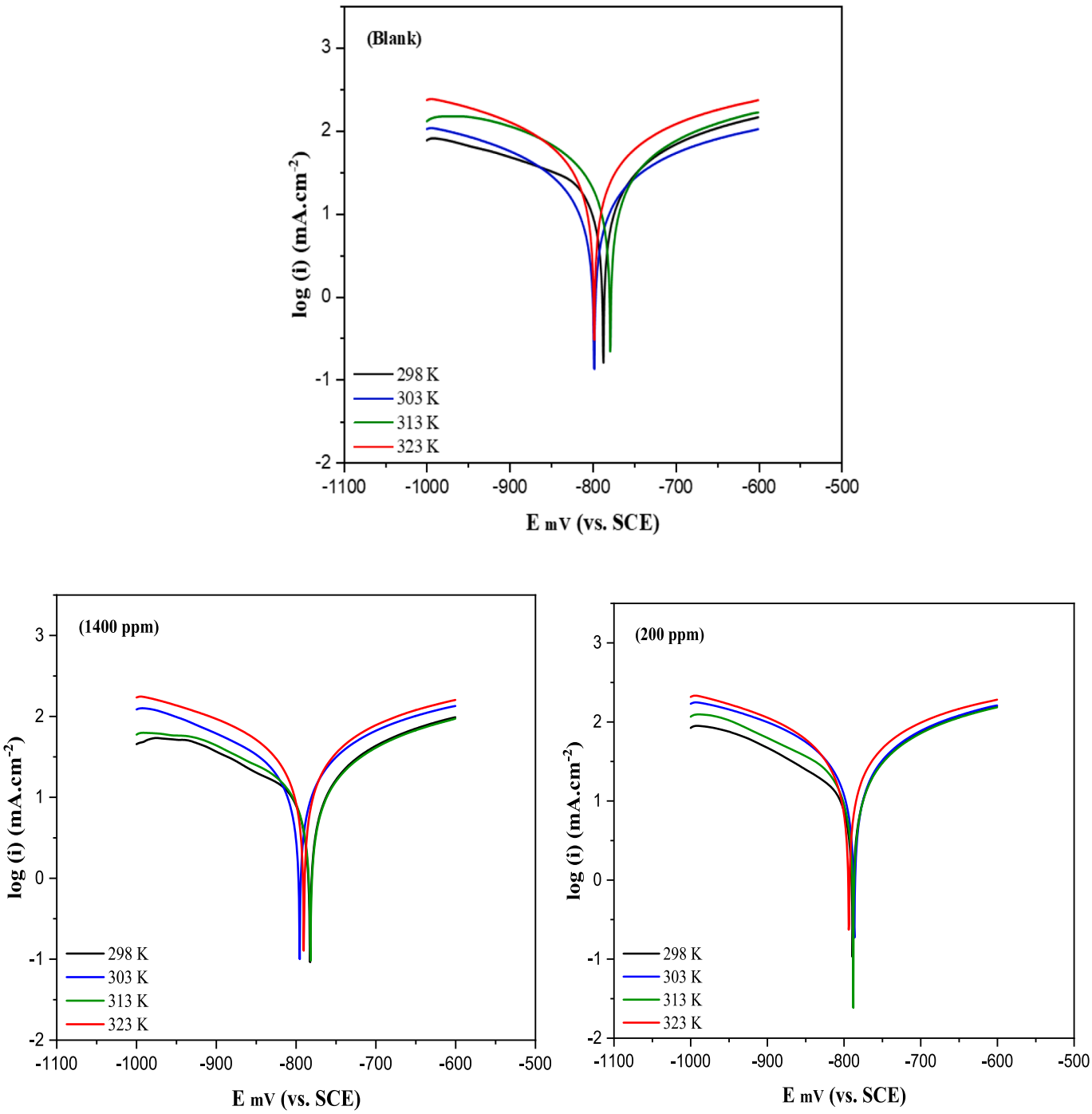

Fig. 7. PDP curves of aluminum immersed in 1 M HCl in the presence and absence of different concentrations of CRD at various temperatures.

activation enthalpy as shown in Table 2 indicates that the addition of the inhibitor in solution constitutes a barrier to the corrosion reaction. The almost similar values in E_a and ΔH_a^0, which are higher in the presence of CRD, reveal that Al's dissolution process remained unchanged due to the increase of the energy barrier (Abdelhadi et al., 2023).

The entropy decreases negatively in the presence of CRD because of the disorder decrease of the water molecules during the transformation from reactive into an active complex of inhibitor and metal (Fouda et al., 2014; Rugmini Ammal et al., 2018) which generates a displacement of several water molecules of the inhibitor (Shainy et al., 2016). Thus, a stable layer has been created on the surface of aluminum (Arrousse et al., 2022). The inhibitor progresses with the same way of the enthalpy and the activation energy (Zarrouk et al., 2011). An increase in EI(%) with temperature combined with a smaller E_a for the V_{corr} in the presence of the inhibitor points to a specific interaction between the Al surface and the inhibitor in HCl solution (Fouda et al., 2012).

3.5. Adsorption isotherm and thermodynamic parameters

Understanding the adsorption characteristics of inhibitor molecules on electrode surfaces is crucial, which involves analyzing the adsorption mechanism through isotherm and thermodynamic parameters. The type of adsorption is discernible from the adsorption energy of the inhibitor molecules. Typically, physical adsorption occurs through weak Van der Waals forces that facilitate reversible bonding between the metal surface

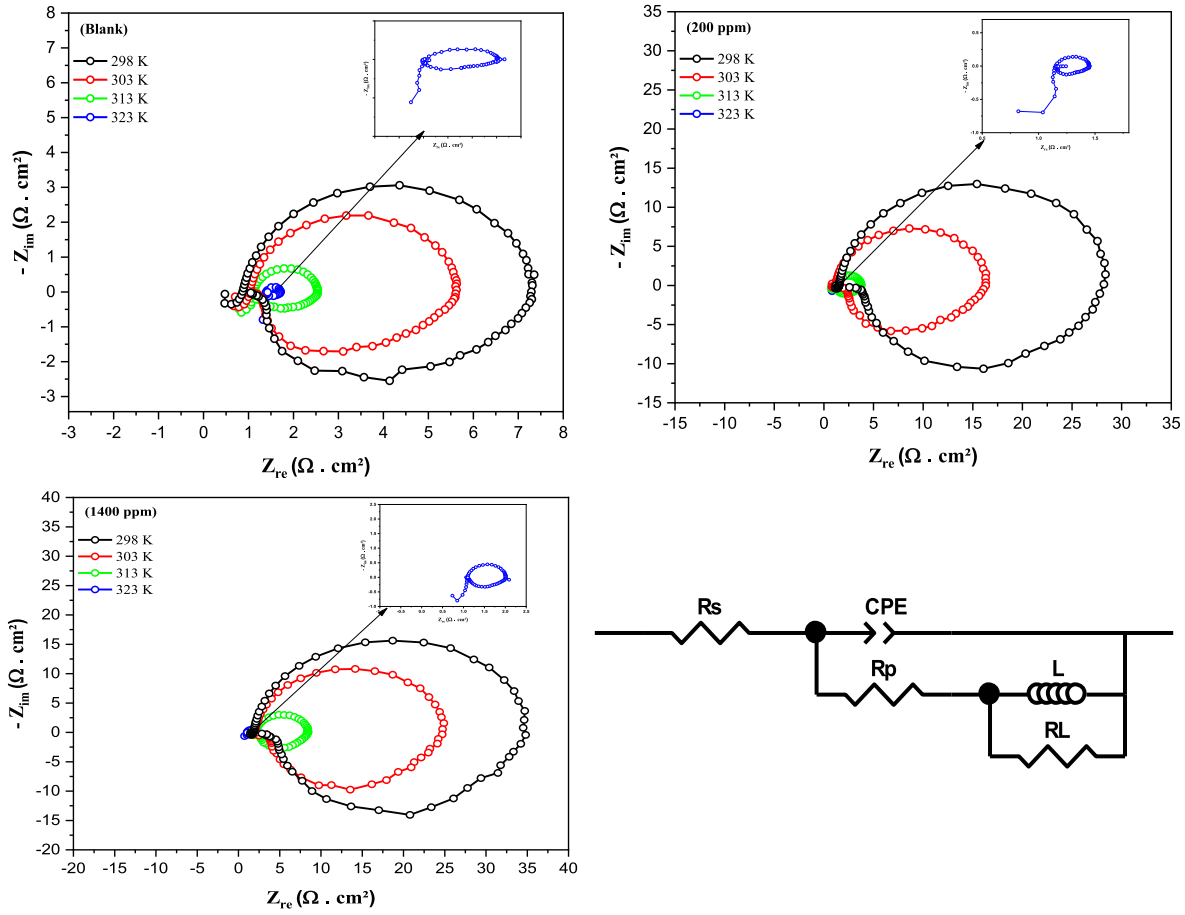

Fig. 8. Electrical equivalent circuit model and aluminum Nyquist diagrams in HCl without and with CRD concentrations at various temperatures.

and the inhibitor molecules. In contrast, chemical adsorption involves the formation of stronger ionic or covalent bonds between the inhibitor molecules and the metal surface, indicating a more permanent interaction (Tezcan et al., 2018). The interaction between the inhibitor molecule and the metal surface is well-characterized by the adsorption isotherm, which establishes the precise contact mechanism. The choice of the most appropriate isotherm model is guided by the best fit to our experimental data, as indicated by the highest correlation coefficient (R^2). We examined various models, including the Langmuir, Temkin, Freundlich, and Frumkin adsorption isotherms. The adsorption parameters are presented in Table 3, and the plots of adsorption CRD on aluminum were fitted and are presented in Fig. 6. All data are expressed in their linear forms to facilitate the analysis of adsorption thermodynamics (Eqs. (24)–(27)):

Langmuir:

$$\frac{C_{inh}}{\theta} = \frac{1}{K_{ads}} + C_{inh} \tag{24}$$

Temkin

$$\theta = ln(C_{inh}) + K_{ads} \tag{25}$$

Freundlish

$$exp(f\theta) = K_{ads}C_{inh} \tag{26}$$

Frumkin

$$\frac{\theta}{1-\theta} exp(-2f\theta) = K_{ads}C_{inh} \tag{27}$$

where C_{inh} denotes the concentration of the inhibitor, while θ indicates the surface coverage. The term (f) is used to represent the factor of energetic inhomogeneity, and K_{ads} stands for the adsorption equilibrium constant. Our investigation revealed that the Langmuir isotherm model, which provided the most accurate description, demonstrated uniformity with a regression value ($R^2 = 0.997$). This suggests a single layer of adsorption onto the mild steel surface without lateral interactions between adsorbed species. The assumption of monolayer adsorption explains this good linearity (Hussin et al., 2016). Gibb's free energy, calculated using Eq. (28), quantifies the thermodynamic spontaneity of adsorption, elucidating the energetic feasibility of the adsorbate-adsorbent interaction.

$$\Delta G^0_{ads} = -R \times T \times \ln(55.5 Kads) \tag{28}$$

In this context, K_{ads} denotes the adsorption equilibrium constant, while 55.5 represents the molar concentration of water. R is the universal gas constant, and T is the temperature in Kelvin, denoted as K. A higher K_{ads} value typically indicates stronger adsorptive interactions (Li et al., 2022), which often correlates with higher corrosion inhibition efficiency. The equilibrium constant (K_{ads}) of 0.9057 L/mol in our study reflects strong adsorption, while the negative Gibbs free energy change ($\Delta G^0_{ads} = -9.73$ kJ/mol) confirms the spontaneity of the adsorption process. Notably, the ΔG^0_{ads} value being less negative than −20 kJ/mol often indicates a predominance of physical adsorption involving weak electrostatic interactions between the inhibitor molecules and the electrode. However, values approaching or exceeding −40 kJ/mol would suggest a chemical adsorption mechanism, which involves the formation of stronger covalent or coordination bonds. Given our ΔG^0_{ads} value, the adsorption is likely physical (Hussin et al., 2016; Li et al., 2022). These findings provide crucial insight into the thermodynamic

Table 4
EIS parameters of aluminum in 1 M HCl without and with CRD concentrations at various temperatures.

Inhibitor	*Temperature (K)*	R_s (Ω.cm^2)	R_p (Ω.cm^2)	R_L (Ω.cm^2)	*CPE*		R_{ct} (Ω.cm^2)	*L* (*H.cm^2*)	X^2	η_{EIS} %
					$Q.10^5$ (Ω^{-1}. S^n.cm^{-2})	*n*				
Blank	*298*	0.93	0.332	5.705	3.37	0.98	6.037	1.392	0.0019	-
	303	1.09	0.183	4.067	0.391	0.99	4.250	0.864	0.001	–
	313	1.16	0.04	1.243	4.74	0.99	1.283	0.173	0.001	–
	323	1.12	0.051	0.16	7.9	0.99	0.211	0.016	0.00009	–
CRD	*298*	1.58	2.254	23.43	6.74	0.97	33.04	4.38	0.0007	86.05
200 ppm	*303*	1.255	0.751	13.29	4.69	0.98	14.041	2.247	0.001	75.06
	313	1.12	0.09	2.358	5.34	0.99	2.448	0.37	0.0007	55.5
	323	1.11	0.1	0.226	26.5	0.93	0.854	0.029	0.0002	49
CRD	*298*	1.88	2.649	29.27	5.6	0.97	33.04	6.086	0.0008	87.5
1400 ppm	*303*	1.47	1.272	14.08	0.69	0.97	15.352	2.62	0.0003	85.6
	313	2.14	0.184	5.758	6	0.99	5.942	0.95	0.0003	78.3
	323	1.13	0.13	0.746	5.7	0.99	0.854	0.068	0.001	60.8

Table 5
Potentiodynamic polarization parameters from Tafel plots of aluminum in 1 M with and without the addition of CRD inhibitor.

Inhibitor	*Temperature (K)*	E_{corr} vs. Ag/AgCl (mV)	i_{corr} (mA.cm^2)	βa (mV.dec^{-1})	βc (mV.dec^{-1})	*θ*	η_p %
Blank	*298*	−785.3	62.97	318.5	−658.3	–	–
	303	−776.9	72.1	486.6	−550	–	–
	313	−795	88.3	755.2	−679.9	–	–
	323	−796.4	106.4	1107.7	−943.2	–	–
CRD	*298*	−786.9	11.17	110.4	−175.2	0.8226	82.26
200 ppm	*303*	−786.2	19.2	162.1	−217.7	0.7337	73.37
	313	−784.9	43.4	312.4	−312.1	0.5084	50.84
	323	−792	55.85	347.5	−327.8	0.4751	47.51
CRD	*298*	−780.9	8.6	127.2	−186	0.8634	86.34
1400 ppm	*303*	−780	11.41	145.3	−201.9	0.8417	84.17
	313	−793.8	20.38	184.2	−217.8	0.7691	76.91
	323	−788.6	41.5	303.9	−306.6	0.6099	60.99

viability and the nature of corrosion inhibition under the studied conditions.

3.6. Electrochemical measurements

3.6.1. Potentiodynamic polarization curves

To examine the behavior of aluminum in the presence and absence of CRD, potentiodynamic polarization analyses were conducted in a 1.0 mol/L HCl medium. Fig. 7 presents the Tafel curves recorded for CRD concentrations of 200 ppm and 1400 ppm at various temperatures ranging from 298 to 323 K. Table 4 displays the kinetic parameters obtained by extrapolating the linear portions of the anodic and cathodic branches to the corrosion potential, specifically the corrosion current density. The recorded parameters, including corrosion rate (i_{corr}), corrosion potential (E_{corr}), cathodic and anodic Tafel slopes (βc and βa), and inhibition efficiency (η_p%) for different CRD concentrations in a 1 mol/L HCl medium, are summarized in Table 5. The presence of an inhibitor results in a noteworthy decrease in current density values, eventually reaching levels lower than those observed in the uninhibited solution. This effect becomes more pronounced with increasing CRD doses from 200 to 1400 ppm. In acidic solutions, the concentration of H^+ ions is sufficiently high, resulting in the removal of oxygen from the solution. Consequently, the primary anodic reaction involves the dissolution of aluminum in the form of Al^{3+} aqueous complexes and their migration from the metal surface into the solution. Simultaneously, the primary cathodic reaction entails the reduction of hydrogen ions and the generation of hydrogen gas (Halambek and Berković, 2012). According to previous literature, A compound can be classified as either an anodic-type or a cathodic-type inhibitor if the difference in the E_{corr} value exceeds 85 mV (Al-Amiery et al., 2018). As CRD exhibited a maximum deviation of 9 mV from the aluminum potential in the control solution, it suggests that CRD acted as a mixed-type inhibitor. This result may suggest that the inhibition primarily took place through the obstruction of available cathodic and anodic sites on the metal surface, achieved through the adsorption of inhibitor molecules onto the aluminum surface. The small shift in the Tafel slopes when inhibitors were used indicates that the inhibitors worked by blocking the metal's reaction sites on the surface, without changing how the anodic and cathodic reactions occur (Verma et al., 2023).

3.6.2. Electrochemical impedance Spectroscopy (EIS)

After achieving a stable equilibrium of the potential at the interface between the metal and the solution using the OCP technique, the electrochemical impedance spectroscopy (EIS) technique was conducted to comprehend the mechanisms behind corrosion inhibition reactions, both in the absence and presence of CRD concentrations at various temperatures ranging from 298 to 323 K. Fig. 8 illustrates the Nyquist data plot obtained during the analysis in a 1 mol/L HCl solution. The impedance spectra exhibit capacitive loops at higher frequencies and inductive loops at lower frequencies. The presence of a depressed semicircle in the Nyquist plot throughout the examined frequency range suggests that the corrosion of aluminum is primarily governed by a charge transfer process. Similar observations in the literature have been documented for the corrosion of aluminum alloys in HCl solutions (Zhao et al., 2017). The inductive loop is typically associated with the relaxation process in the oxide film covering the metal surface (Reena Kumari

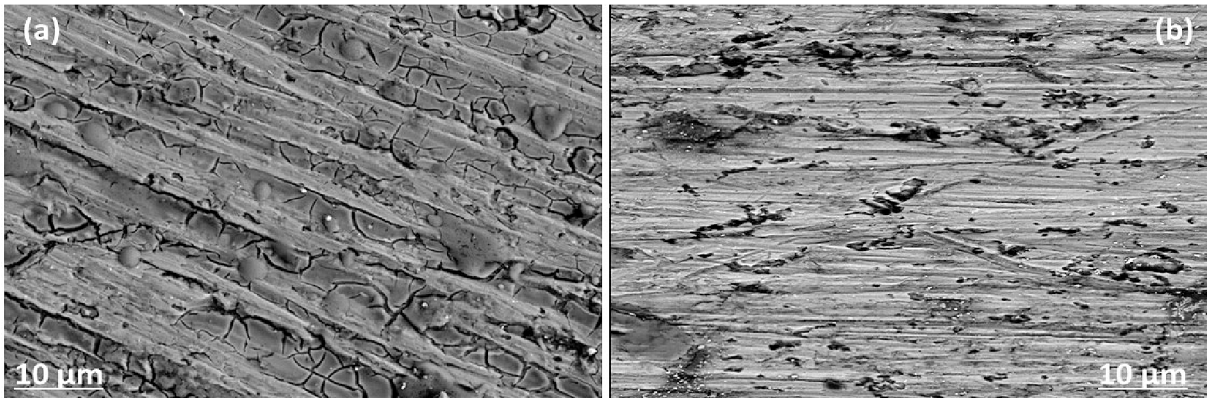

Fig. 9. SEM micrographs of aluminum surface after 4 h immersion in 1.0 mol/L HCl without (a) or with 1000 ppm of CRD (b).

et al., 2016).The high-frequency capacitive loop may also be linked to the presence of the oxide layer on the aluminum surface. Therefore, this loop can be associated with the dielectric properties of the complex formed (Halambek and Berković, 2012). Deviations from perfect semicircles are usually due to the frequency dispersion of interfacial impedance, which can be attributed to various physical phenomena such as active sites, surface roughness, and non-uniformity of the solids (Mohsenifar et al., 2016). The spectra demonstrate that impedance undergoes rapid changes as the inhibitor concentration varies. The recorded impedance values rise as the inhibitor concentration increases, suggesting enhanced protection of the metal surface (Al Otaibi and Hammud, 2021).

Based on AC circuit theory, the experimental data were simulated using the equivalent electric circuit presented in Fig. 8, enabling the correlation between impedance plots and equivalent circuits. The reliability of the fit was confirmed by examining the chi-squared element, χ^2. The EIS parameters, including electrolyte resistance (R_s), polarization resistance (R_p), inductive resistance (R_L), constant phase element (Q; n), and the double layer capacitance (C_{dl}), are documented in Table 5. Instead of employing an ideal capacitor, a Constant Phase Element (CPE) was used (Li et al., 2015). C_{dl} values, and the impedance for CPE, denoted as Z_{CPE}, are calculated using the following equations (Thoume et al., 2021):

$$C_{dl} = (Q \times R_p^{1-n})^{\frac{1}{n}} \quad (29)$$

$$Z_{CPE} = \mathrm{Q}^{-1} \times (i \times \omega)^{-n} \quad (30)$$

where i represents the imaginary unit, Q is the CPE constant, ω stands for angular frequency, and n denotes the phase shift behavior that characterizes the metal's inhomogeneity. The progressive increase in R_p values with the addition of different concentrations of the CRD inhibitor results in a systematic improvement in inhibitory efficiency, reaching 87.5 % with 1400 ppm of CRD. It's important to note that all the systems studied yield n values close to 1, indicating a predominant capacitive behavior. The increase in charge transfer resistance (R_{ct}) values and the decrease in Constant Phase Element (CPE) values with rising inhibitor concentrations suggest the development of a protective layer on the electrode surface. This layer serves as a barrier to both mass and charge transfer (Soltani et al., 2016). Resulting in a slowly corroding system, this is attributed to the gradual displacement of water molecules by inhibitor molecules on the surface, consequently reducing the number of active sites for the corrosion reaction (Ahmed et al., 2018). This leads to the conclusion that the CRD inhibitor serves as an effective protective coating against hydrochloric acid.

3.7. Scanning electron microscopic measurement (SEM)

The SEM technique was used to examine the morphology of the surface layer of the Al alloy in inhibited and uninhibited mediums. The metal was immersed for 4 h in 1.0 mol/L HCl with and without adding 1000 ppm of inhibitor. In the absence of inhibitor, the corrosive HCl solutions attack the aluminum surface, causing significant damage (Fig. 9). The surface appears smooth, with some abrading scratches caused by abrasive paper. However, it is not completely smooth and uniform, and there are small crevices or scales that can be attributed to an aluminum defect and most probably an oxide inclusion. After 4 h of immersion in a blank 1.0 mol/L HCl solution, the aluminum surface was severely uniformly damaged and completely covered with thick corrosion products. The corroded layer is rough and porous, with some black holes. The aggressive ions can penetrate deep into the fresh Aluminum via these black holes. In contrast, after immersion in HCl solution for 4 h with 1000 ppm CRD, aluminum showed little damage and a relatively even surface (Fig. 9(b)). There are almost no visible covered corrosion products, and some original abrasive paper abrading scratches can still be seen on the aluminum surface, indicating the effective inhibition ability of CRD. In comparison to (Fig. 9(a)), there is a good protective film formed by CRD adsorption on the surface, which shields the aggressive ions from attacking the metal surface.

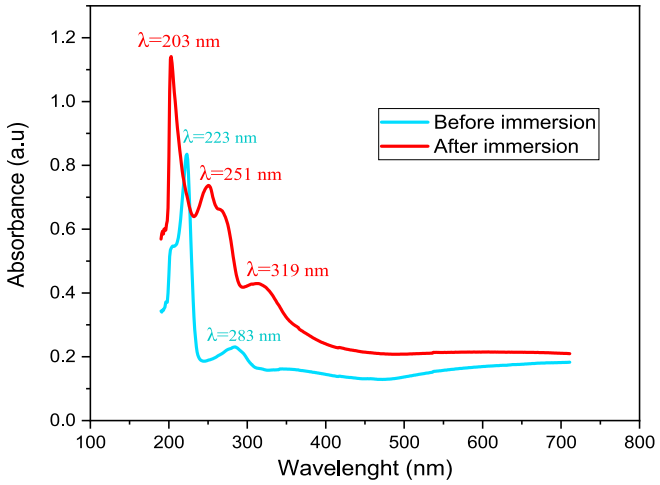

Fig. 10. UV–visible spectra of the aluminum in the presence of CRD before and after immersion in 1.0 mol/L HCl.

3.8. Spectroscopic studies

Spectrometry analysis was performed to further understand the interaction between Al and the CRD used. The UV–visible absorption spectra of the RC, 1.0 mol/L HCl solution studied before and after the corrosion test (Fig. 10) was carried out in order to detect the presence of

Table 6
Values of the operating parameters used at different levels.

Real variables	Units	Centered variables	Low level		Central point	High level	
			−1.68	−1	0	1	1,68
CRC	(ppm)	x1	200	443.24	800	1156.76	1400
T	(°C)	x2	5	16.15	32.5	48.85	60
t_I	(h)	x3	1	1.61	2.5	3.39	4

Table 7
Matrix of tests for the inhibition of aluminum corrosion in HCl medium established by RSM.

N°	Coded variables			Real variables		
	CRC (ppm)	T (°C)	t_I (h)	CRC (ppm)	T (°C)	t_I (h)
1	0	0	0	800	32.5	2.5
2	−1	−1	−1	443.24	16.15	1.61
3	1	−1	−1	1156.76	16.15	1.61
4	−1	1	−1	443.24	48.85	1.61
5	1	1	−1	1156.76	48.85	1.61
6	−1	−1	1	443.24	16.15	3.39
7	1	−1	1	1156.76	16.15	3.39
8	−1	1	1	443.24	48.85	3.39
9	1.68179	0	0	1400	32.5	2.5
10	0	1.68179	0	800	60	2.5
11	0	0	1.68179	800	32.5	4
12	0	0	0	800	32.5	2.5

organic compounds and identify the possible adsorption of inhibitor molecules on the Aluminum surface. According to the literature, changing the value and position of the maximum absorbance peak in the UV–visible spectrum indicates the formation of a complex compound between a metal and an inhibitor (Ismail et al., 2022).

The electronic absorption spectra of the inhibitor under study (Fig. 10) before the aluminum immersion display three bands. The first band at λ = 223 nm can be attributed to the medium energy π-π* transition of the aromatic ring, while the second band at λ = 283 nm is due to the low energy π-π* transition. The third band λ = 340 nm is due to the π-π* excitation of the azo group electrons. On the other hand, after the aluminum immersion in the test solution for 4 h, the changes are more significant. The two maxima absorption peaks shifted to 203 nm and 251 nm, respectively. Such changes in both the position of the absorption maxima and the absorbance values indicate that different compounds present in the CRD do not react in the same way with the metal surface during the corrosion process (Deyab and Guibal, 2020), which also confirms the formation of complexes between the species present in solution (Ali and Mahrous, 2017). These experimental results underline the formation of the complex between the Al and CRD molecule.

Table 9
Responses of experimental design tests of inhibition of aluminum corrosion in HCl medium.

N°	CRD (ppm)	T (°C)	t_I (h)	Resp. 1: V_{corr} (mg/cm^{2}h)	Resp. 2: EI(%)
1	800	32.5	2.5	0.2	0.80
2	443.24	16.15	1.61	0.26	0.70
3	1156.76	16.15	1.61	0.37	0.94
4	443.24	48.85	1.61	25.34	66.94
5	1156.76	48.85	1.61	25.09	66.12
6	443.24	16.15	3.39	0.28	1.57
7	1156.76	16.15	3.39	0.16	0.93
8	443.24	48.85	3.39	18.07	0
9	1400	32.5	2.5	0.61	2.40
10	800	60	2.5	24.67	0
11	800	32.5	4	0.18	1.11
12	800	32.5	2.5	0.2	0.80

3.9. Analysis and optimization based on RSM methodology

3.9.1. Evaluation of regression model

Using CCD scheme and through the RSM approach, we have examined the CRD inhibitory effect on the values of V_{corr} of aluminum in a solution of 1.0 mol/L HCl. Optimization studies are essential tools in corrosion systems. RSM is a statistical technique often used in furthermost studies involving modeling and optimization. This method makes it possible to better anticipate (with good accuracy) the effect of the three main independent variables (T, t_I, CRD) on the inhibition efficacy and the corrosion rate as responses. The levels of the factors and their correspondences in reduced-centered variables (Table 6), as well as the matrix of the experiments (Table 7).

- The points −1 and +1: are, respectively, the low and high levels of the CCD plan, the center of the domain is represented by 0.
- The points −1.68 and +1.68 are respectively the low and high levels of the axial points.

Based on the CCD design, ANOVA analysis of variance showed that the quadratic models were suitable for the analysis of experimental data, as shown in Table 8. ANOVA analysis has been used as a consistent method to estimate the corrosion related to the effects of parameters in different fields of scientific and industrial studies (Gaber et al., 2020). The importance of the used model was determined by the calculation of

Table 8
Results of the ANOVA analysis for the corrosion rate (V_{corr}) and inhibition efficiency (EI(%)) of Al in HCl medium.

Source	Df	V_{corr}	EI(%)	V_{corr}	EI(%)	V_{corr}	EI(%)	V_{corr}	EI(%)
		Sum of squares		Mean Square		F-Ratio		P-Value	
A: CRC	1	27.4679	134.948	27.4679	134.948	1.77	1.91	0.3153	0.3007
B: T	1	553.948	1027.91	553.948	1027.91	35.60	14.58	0.0270	0.0622
C: t_I	1	100.289	3087.56	100.289	3087.56	6.45	43.80	0.1264	0.0221
AA	1	19.8538	106.46	19.8538	106.46	1.28	1.51	0.3759	0.3441
AB	1	15.0891	71.3069	15.0891	71.3069	0.97	1.01	0.4286	0.4205
AC	1	14.487	69.5693	14.487	69.5693	0.93	0.99	0.4364	0.4252
BB	1	89.2522	204.581	89.2522	204.581	5.74	2.90	0.1389	0.2306
BC	1	64.4821	2342.57	64.4821	2342.57	4.14	33.23	0.1787	0.0288
CC	1	43.1694	1026.37	43.1694	1026.37	2.77	14.56	0.2377	0.0623
Total error	2	31.1189	140.997	15.5594	70.4987				
Total (corr.)	11	1448.71	7178.62						

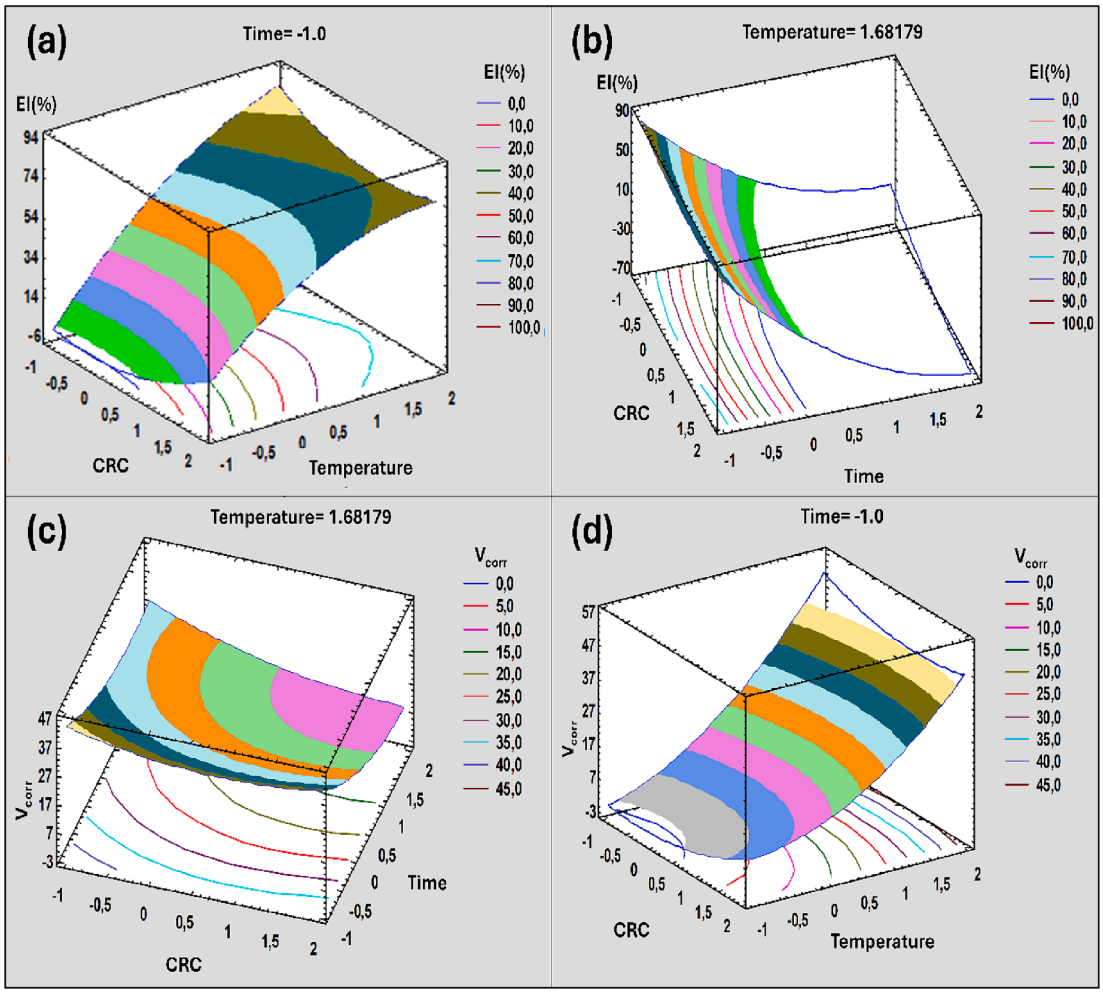

Fig. 11. Variation of inhibition efficiency and corrosion rate in the plan: Inhibitor concentration as a function of temperature ((a) and (b)) and Inhibitor concentration as a function of the duration of immersion ((c) and (d)).

the parameter p ($p < 0.05$). While the adequacy of the model is tested by the coefficient of determination (R squared) in comparison with the adjusted coefficient. The statistic (R^2) designates that the adjusted model explains 97.852 % and 98.0359 % of the variability respectively for the corrosion rate and the inhibition efficacy, which demonstrates a good fit between the expected values and the experimental data (Table 9). Furthermore, (R^2) is reasonably in agreement with the adjusted R-squared statistic of 88.1857 % and 89.1973 % for responses 1 and 2, respectively.

A significant statistical regression model based on the response surface analysis was developed and was also evaluated according to p values ($p < 0.05$). The model equation for corrosion rate is:

$$V_{corr}\ (mg/cm^2\ h) = 0.0663629 - 1.95226*A + 8.76717*B - 3.73037*C + 1.90376*A^2 - 1.62252*A*B - 1.58981*A*C + 4.03646*B^2 - 3.35411*B*C + 2.80724*C^2.$$

Similarly, the final regression model of inhibition efficiency could be expressed using the following equation:

$$EI\ (\%) = 0.51554 - 4.32722*A + 11.9427*B - 20.6982*C + 4.40843*A^2 - 3.52715*A*B - 3.48391*A*C - 6.11116*B^2 - 20.2164*B*C + 13.6881*C^2.$$ C2

where A represents the CRD, B represents *T*, and C is t_I.

3.9.2. *Surface response plots for inhibition efficiency and corrosion rate on aluminum*

The interactive effects of process variables on the V_{corr} and the *EI*(%) were studied by plotting a 3D-dimensional surface curve versus two independent variables, while keeping the other variable constant. The surface curves of the response functions are useful in understanding both the individual and the combined effects between temperature, t_I and CRD (Chung et al., 2021).

The graphs in Fig. 11 indicate the relationship between the factors studied and the responses of the designed experiment. However, (Fig. 11 (a) and (c)) revealed that the EI(%) increases with increasing CRD and increasing the temperature, and thus it indicates that inhibitor concentrations have more effect on the response, but EI(%) decreases with increasing t_I. This may be ascribed to the fact that over the metal remains long in the acid, the more this metal corrodes.

(Fig. 11(b) and (d)) showed that V_{corr} increases with the increase of both parameters, T and t_I. While V_{corr} decreases with the increase in CRD. The RSM was used to analyze responses and to predict the optimal process for the highest values of V_{corr} and EI(%). With the mathematical model of the response surface (contour plot and surface plot), the optimal combination of the factors influencing the aluminum corrosion in HCl solutions has been identified to maximize the values of EI(%). However, according to RSM, the EI(%) will be maximum (81.14 %) if the concentration of CRD inhibitor is maintained at a value of 443.24 ppm for one hour and 37 min of immersion at a temperature of 40 °C.

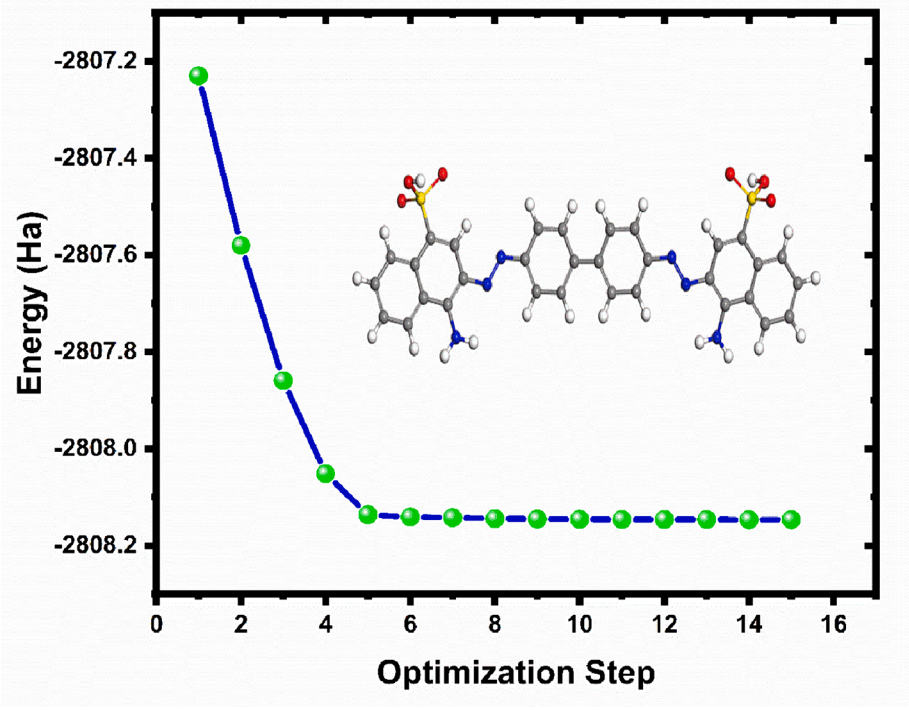

Fig. 12. Energy optimization of CRD calculated by DFT/B3YLP/ DNP method.

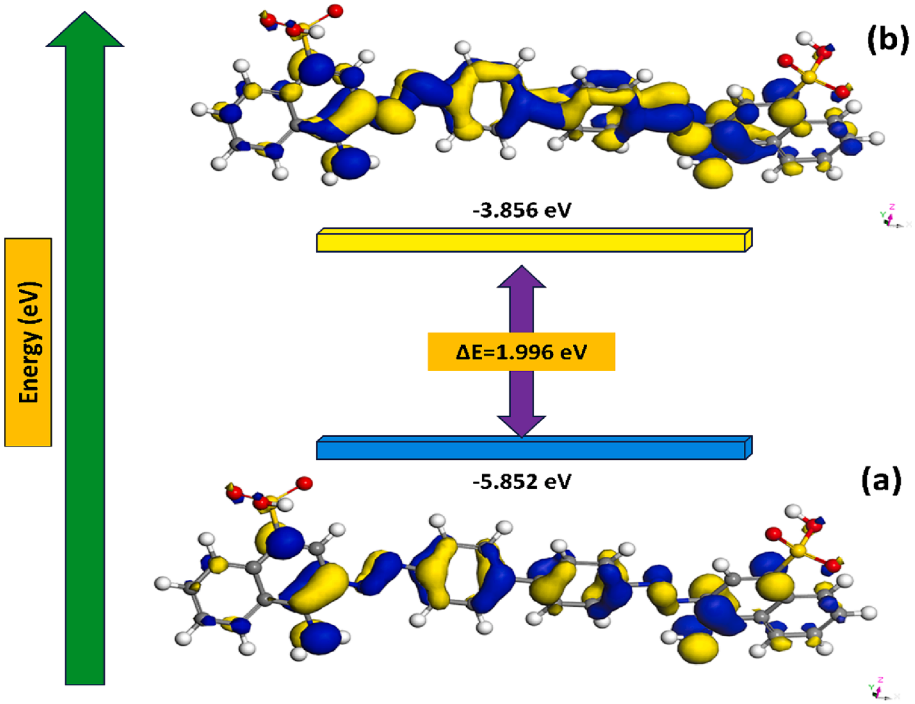

Fig. 13. (a) HOMO (b) LUMO *iso*-surfaces of the CRD molecule obtained by DFT/ B3YLP/DNP method.

3.10. Theoretical analysis

3.10.1. Quantum chemical calculations

The DFT approach was adopted to evaluate the reactivity of the optimized molecular structure of CRD through the calculation of quantum chemical parameters. In comparison to other quantum chemical approaches, it offers several advantages and appears to be sufficient for generating the electronic data required to assess the inhibitory activity of corrosion inhibitors (Haldhar et al., 2021). Figs. 12 and 13 display optimized geometric structure and the frontier molecular orbitals LUMO, HOMO, and molecular electrostatic potential. The values derived from the chemical reactivity descriptors of the investigated inhibitor are summarized in Table 10.

The energy profile represented in Fig. 12 revealed a consistent descent toward a minimum. Commencing at an energy of −2807.2301 Ha, significant conformational adjustments were observed as the energy

Table 10
Calculated theoretical chemical parameters for the CRD inhibitor.

Quantum descriptors		Value
High occupied molecular orbital (eV)	E_{HOMO}	−5.852
Low unoccupied molecular orbital (eV)	E_{LUMO}	−3.856
Energy gap (eV)	ΔE_{gap}	1.996
Ionization potential (eV)	I	5.852
Electron affinity (eV)	A	3.856
Absolute electronegativity	χ	4.854
Global hardness (eV)	η	0.998
Global softness (eV^{-1})	s	1.002
Global electrophilicity index	ω	11.757
Back-donation Energy (eV)	$\Delta E_{Back\text{-}donation}$	0.249
Fraction of electron transferred (eV)	ΔN	−0,813

decreased sharply to −2807.8592 Ha by the third step. As the optimization advanced, diminishing returns in energy reduction emerged, with the transition from step 5 to 15 yielding a subtle change from −2808.1362 Ha to −2808.1467 Ha. The minimal energy difference between the final steps suggests convergence to an optimized geometry, underscoring the effectiveness of the chosen computational approach. Analyzing the electron density plot reveals that, except for the sulfate group in the investigated compound, The CRD molecule's HOMO orbitals are distributed throughout on two benzene rings substituted by SO_3^- groups (containing an attached nitrogen atom). The CRD molecule's LUMO orbitals are found on the sulfur atom, nitrogen atom, and benzene ring, indicating that the inhibitor has a high ability to attract electrons, suggesting that donor–acceptor interactions might influence how this dye is attracted to the adsorbent surface.

The energy of the E_{LUMO}, E_{HOMO}, and ΔE_{gap} = (E_{LUMO} - E_{HOMO}) was explored. The ability of a molecule to donate electrons is typically associated with E_{HOMO}. Inhibition works better with larger E_{HOMO} values. High E_{HOMO} values indicate a molecule's propensity to donate electrons to appropriate acceptor molecules with open, low-energy atomic orbitals. The ability of a molecule to accept electrons is known as E_{LUMO}. The lowest value of E_{LUMO} indicates that the molecule will most likely swiftly accept electrons from donor molecules (Hadisaputra et al., 2022; Qiang et al., 2018). The HOMO (Fig. 13) is characterized by significant electron density localization on the nitrogen atoms and the central aromatic rings, reflecting the molecule's potential for electron donation in chemical interactions. These areas are crucial for interactions with electrophilic agents, as they represent the regions of highest electron density within the molecule. Conversely, the LUMO primarily involves electron density on the oxygen atoms located in the peripheral sulfonic groups and the extended conjugated system. This localization indicates regions where the molecule is most susceptible to electron acceptance, highlighting potential reactive sites for nucleophilic attack. Electrostatic surface potentials (ESP) can be employed to validate the reactive centers of various chemical systems involved in both electrophilic and nucleophilic processes (Azzam et al., 2020). Fig. 14 presents the 3D Electrostatic Surface Potentials of CRD, where yellow regions indicate areas with high potential and blue regions denote areas with low potential. High potential, similar to atomic charges, is concentrated around the functional groups. This figure also provides a 3D visualization of the CRD molecule's electrostatic surface potentials, color-coded to indicate areas of high and low ESP. Regions with high ESP, shown in yellow, typically encompass areas around electropositive atoms such as hydrogen and certain carbon atoms in the molecule. These yellow zones suggest parts of the molecule that are less electron-rich and thus more attractive to electron-donating (nucleophilic).Conversely, areas depicted in blue represent low ESP, indicating a higher electron density. These are often found around electronegative atoms such as oxygen, nitrogen, or the aromatic rings in the molecule. The aromatic rings, due to their delocalized π-electron systems, generally exhibit lower ESP and appear in shades of blue, signaling their potential to attract electron-poor (electrophilic).The energy gap (ΔE_{gap}) makes it possible to compare the reactivity of molecules. The lower ΔE_{gap} is, the better the reactivity of the molecule and vice versa.

According to the value of ΔE (1.996 eV), and compared to many previously reported inhibitors (Ebenso et al., 2021; Lgaz et al., 2021), the CRD is highly reactive and favors the inhibitor's adsorption on the surface of aluminum, which results in a powerful inhibitory effect. A crucial parameter for describing the process of electron transfer from the inhibitor to the metal is the electron transferred fraction (ΔN). While negative values of ΔN signify that electrons move from the metal to the inhibitor molecule, positive values of ΔN show that electrons are moved from the inhibitor to the metal. In the current work, ΔN is positive, and ($\Delta N < 3.6$) suggests that the investigated inhibitor may donate electrons to the Al surface to form coordinated bonds, resulting in the adsorption of an inhibitory layer on the surface (Gupta et al., 2023). In addition, the low values of electronegativity (χ) and Global hardness (η) may help to explain the significant inhibitory power of CRD, which is mostly attributed to its intensive acceptor/donor interactions with Al atoms (Toukal et al., 2018). The global hardness (η) and chemical softness (S) of an organic molecule are essential parameters for determining its reactivity. The (η), which is the inverse of (S), evaluates a molecule's resistance to charge transfer during a chemical process. A hard molecule exhibits higher η and lower S, indicating lower reactivity and greater stability, whereas a soft molecule displays higher S and lower η, indicating higher reactivity and better stability (Cao et al., 2021). According to the results, the global hardness and softness ($\eta = 0.998$ eV; $S = 1.002$ eV^{-1}) indicate that the CRD molecule has a preference for easily exchanging electrons with its environment. This property can promote its adsorption on the surface of the adsorbent (Amrhar et al., 2023). It is also reported that the chemical potential (μ), electronegativity (χ), and electrophilicity index (ω) are chemical reactivity parameters that can reveal the dye adsorption ability on the metal surface (Boumya et al., 2021). Index (ω) is thought to make it possible to determine the

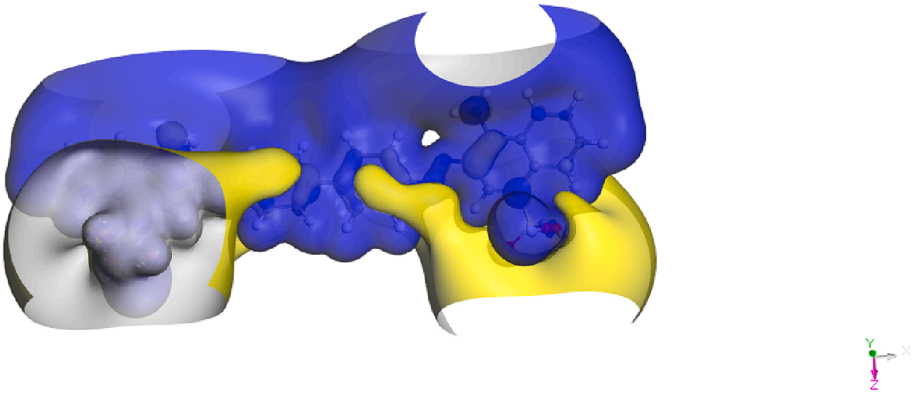

Fig. 14. 3D Electrostatic surface potentials of CRD (high ESP: yellow, low ESP: blue).

Table 11
Calculated Fukui function indices of the CRD by DFT/B3LYB methods.

Atom	f-	f+	f^0
S (1)	0.002	0.001	0.002
S (2)	0.002	0.001	0.002
O (3)	0.013	0.010	0.012
O (4)	0.013	0.010	0.012
O (5)	0.015	0.009	0.012
O (6)	0.022	0.017	0.019
O (7)	0.015	0.009	0.012
O (8)	0.021	0.017	0.019
N (9)	0.037	0.017	0.027
N (10)	0.037	0.017	0.027
N (11)	0.008	0.054	0.031
N (12)	0.008	0.054	0.031
N (13)	0.014	0.038	0.026
N (14)	0.014	0.038	0.026
C (15)	0.002	0.011	0.006
C (16)	0.002	0.011	0.006
C (17)	0.004	0.002	0.003
C (18)	0.003	0.002	0.003
C (19)	0.024	0.008	0.016
C (20)	0.024	0.008	0.016
C (21)	0.015	0.023	0.019
C (22)	0.015	0.023	0.019
C (23)	0.028	−0.008	0.010
C (24)	0.029	−0.008	0.010
C (25)	0.000	0.010	0.005
C (26)	0.000	0.010	0.005
C (27)	0.010	0.003	0.007
C (28)	0.010	0.003	0.007
C (29)	0.009	0.009	0.009
C (30)	0.009	0.009	0.009
C (31)	0.013	0.018	0.016
C (32)	0.013	0.018	0.016
C (33)	0.011	0.007	0.009
C (34)	0.011	0.007	0.009
C (35)	0.010	0.013	0.012
C (36)	0.010	0.013	0.012
C (37)	0.014	0.007	0.011
C (38)	0.014	0.008	0.011
C (39)	0.009	0.005	0.007
C (40)	0.009	0.005	0.007
C (41)	0.008	0.011	0.010
C (42)	0.008	0.011	0.010
C (43)	0.010	0.018	0.014
C (44)	0.010	0.018	0.014
C (45)	0.011	0.011	0.011
C (46)	0.011	0.011	0.011

electrophilic tendency of a molecule. It must be noted that the greatest value is 4.854 eV for CRD. This indicates that the inhibitor exhibits greater inhibitory action. The chemical potential (μ) is related to the molecule's inhibitory effects and is attributed to its polarity. An increased dipole moment enhances the adsorption of inhibitory chemicals onto the metal surface (Salman, 2020; Al-Azawi et al., 2016).

On the other hand, the ability of a chemical species to attract electrons is characterized by electronegativity, which is the negative of chemical potential ($\chi = -\mu$) (Saraçoğlu et al., 2018). The ability of a molecule to attract electrons is reflected in its electrophilicity (Pucci and Angilella, 2022). The tendency to take electrons is linked with the electrophilicity of the chemical system and the associated molecule with a high value of χ and ω. Conversely, a molecule having a low value of χ and ω indicates an electron-donating capacity with nucleophilicity (Abad et al., 2020; Parlak et al., 2022). It is important to note that the nitrogen and oxygen atoms of the studied inhibitor each have a single electron pair and a π-delocalized bond. Through electron exchange, this provides the inhibitor molecule on the surface of aluminum with chelating efficacy.

3.10.2. Local reactivity of the corrosion inhibitor

The Fukui indices were used to investigate the regions of local reactivity of the investigated inhibitor compound, which provides information about the atoms in a molecule that have a greater tendency to either lose or receive electrons. These indices identify the reactive areas of molecules in terms of electrophilic, nucleophilic, and radical attacks. Inhibitor molecules can bind to the metal surface through electron transfer, electrostatic attraction, or a combination of both. Therefore, it is critical to examine the active site of these interactions and explain their nature and processes. The calculated Mulliken atomic charge distribution is presented in Table 11.

In analyzing the Fukui function for radical attacks (f^0), which measures the change in electron density when an electron is added or removed from a inhibitor, it is evident that nitrogen atoms N (9) and N (10) of CRD display significant radical reactivity with f^0 values of 0.027. This suggests their critical role in interacting with radicals during the corrosion process, potentially enhancing the inhibitor's protective efficiency. Oxygen atoms such as O (6) and O (8), with f^0 values of 0.019, also demonstrate substantial reactivity, indicating their ability to stabilize radical intermediates. Carbon atoms, like C (23) and C (24), though less reactive with f^0 values of 0.010, contribute to the molecule's overall stability and effectiveness in corrosion inhibition.

The $f+$ measure denotes density changes when molecules accept electrons and corresponds to reactivity towards nucleophilic attacks. Conversely, f^- signifies reactivity with respect to electrophilic attacks or when the molecule loses electrons. As shown in Fig. 15, The largest value of f^+ which is responsible for accepting electrons from the Aluminum surface is located on the N (11) and N(12) and N(13) atoms of molecule inhibitor while the largest value of f^- in charge of donating electrons to the Aluminum surface are atoms and N(9) and N(10) and C(23) and C (24). The results obtained show that all nitrogen atoms in the –N=N– group, associated with the centers of the fused aromatic rings, are suitable targets for nucleophilic and electrophilic attacks. Their tendency to donate or accept electrons suggests that the investigated compound are effective corrosion inhibitors (Pareek et al., 2019). The calculated Fukui indices and the electron density distribution in the HOMO and LUMO orbitals of the inhibitor compound show a strong alignment. The results affirm the presence of analogous reactive zones on the aluminum surface for both nucleophilic and electrophilic attacks.

3.10.3. MD simulations

Molecular Dynamics (MD) simulations serve as a valuable theoretical tool for exploring the interactions between corrosion inhibitors and metal surfaces. Herein, the MD simulations were carried out to provide a better understanding of the adsorption configurations and interactions of Congo Red Dye (CRD) on the Al (1 1 0) surface. Fig. 16 presents both top and side views of the final MD snapshots, showcasing the adsorption of a single CRD molecule onto the Al (1 1 0) surface. These views highlight that CRD adopts a flat-type molecular orientation, positioning itself parallel to and close to the aluminum surface. This proximity allows the active centers of the dye molecules to efficiently interact with the Al surface, potentially enhancing its protective effectiveness. Further analysis of the MD simulations reveals that the binding energy of the CRD adsorption process is 213.55 kcal/mol. This high binding energy indicates a strong attractive force between the inhibitor and the metal surface, which correlates with a higher inhibition efficiency. This positive energy value underscores the CRD's spontaneous and effective interaction capability with the Al (1 1 0) surface (Verma et al., 2018; Zhao et al., 2017).

The simulations predict that in this arrangement, the inhibitor molecule will have robust interactions with the surface, offering multiple avenues for both chemical and physical interactions between the active sites of the dye and the metal atoms. These theoretical findings align with the experimental results, indicating that CRD is an effective inhibitor of aluminum corrosion.

4. Conclusion

The study investigated the corrosion inhibition and adsorption

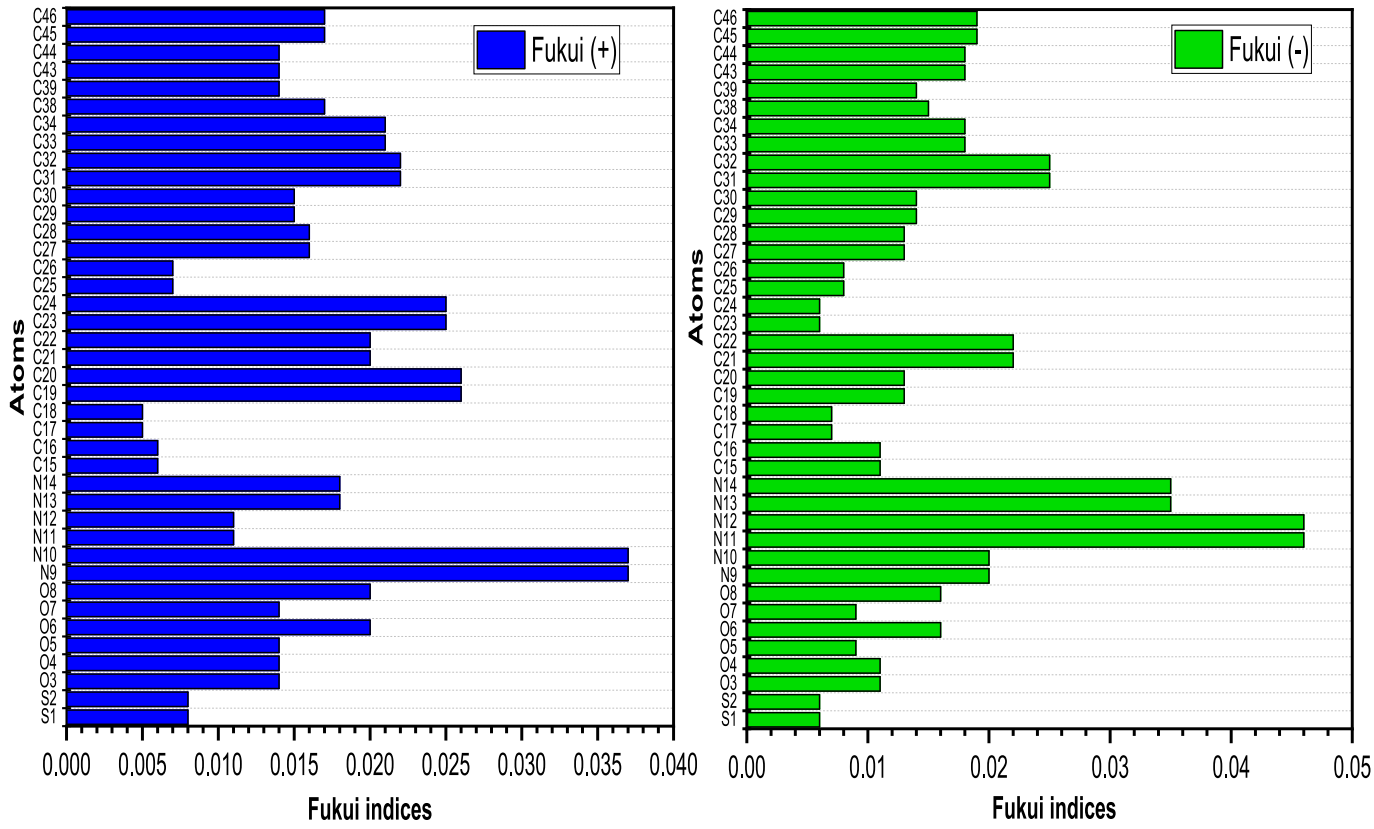

Fig. 15. Graphical illustration of the Fukui function indices for selected atoms in the investigated inhibitor.

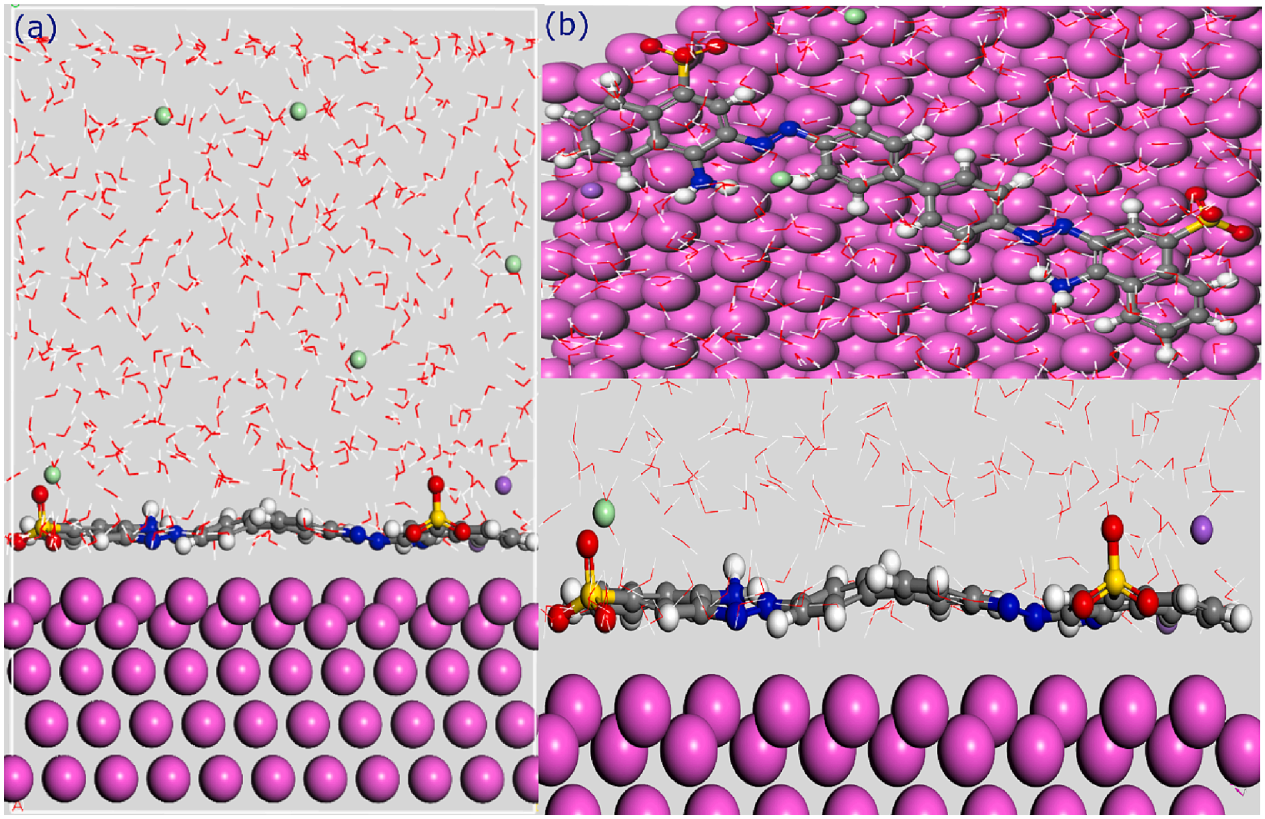

Fig. 16. The most stable adsorption configuration of CRD molecule on the Al(1 1 0) surface obtained from MD simulation.

properties of CRD in a 1 mol/L HCl solution using a combination of experimental techniques and a theoretical approach. The main conclusions are as follows:

- CRD acts as an efficient inhibitor for aluminum corrosion in a 1 mol/L HCl acidic medium, with an inhibition efficiency of 87.5 % confirmed by PDP results.
- The results from both the weight loss and EIS techniques exhibited strong consistency, with the efficiency of inhibition (EI %) increasing alongside CRD concentration.
- SEM and UV–Vis analyses revealed the formation of a protective film on the aluminum surface in the inhibited system.
- Statistical analysis shows that the quadratic model is statistically acceptable, with R^2 values of 97.852 % and 98.0359 % for the corrosion rate and the inhibition efficacy, respectively. The optimized results obtained through RSM indicate an optimal inhibition efficiency of 81.14 % in the HCl solutions.
- DFT, in combination with theoretical observations from MC/MD simulations, suggests the stable adsorption of the inhibitor molecule onto the aluminum surface.

CRediT authorship contribution statement

Ayoub Chahid: Formal analysis, Data curation, Writing – original draft. **Mohammed Chafi:** Conceptualization, Methodology, Resources, Supervision, Writing – review & editing. **Mohamed Essahli:** Conceptualization, Methodology, Resources, Supervision, Writing – review & editing. **Awad A. Alrashdi:** Investigation, Software, Validation, Writing – review and editing. **Hassane Lgaz:** Investigation, Software, Validation, Writing – review and editing.

Declaration of competing interest

The authors declare that they have no known competing financial interests or personal relationships that could have appeared to influence the work reported in this paper.

References

Abad, N., Lgaz, H., Atioglu, Z., Akkurt, M., Mague, J.T., Ali, I.H., Chung, I.-M., Salghi, R., Essassi, E.M., Ramli, Y., 2020. Synthesis, crystal structure, hirshfeld surface analysis, DFT computations and molecular dynamics study of 2-(benzyloxy)-3-phenylquinoxaline. J. Mol. Struct. 1221, 128727 https://doi.org/10.1016/j.molstruc.2020.128727.

Abboud, Y., Abourriche, A., Saffaj, T., Berrada, M., Charrouf, M., Bennamara, A., Hannache, H., 2009. A novel azo dye, 8-quinolinol-5-azoantipyrine as corrosion inhibitor for mild steel in acidic media. Desalination, Issue 1: Water Resources Management: New Approaches and Technologies 237, 175–189. https://doi.org/10.1016/j.desal.2007.12.031.

Abbout, S., Hsissou, R., Erramli, H., Chebabe, D., Salim, R., Kaya, S., Hajjaji, N., 2021. Gravimetric, electrochemical and theoretical study, and surface analysis of novel epoxy resin as corrosion inhibitor of carbon steel in 0.5 M H2SO4 solution. J. Mol. Struct. 1245, 131014. https://doi.org/10.1016/j.molstruc.2021.131014.

Abdallah, M., Atwa, S.T., Zaafarany, I.A., 2014. Corrosion inhibition of aluminum in NaOH solutions using some bidentate azo dyes compounds and synergistic action with some metal ions. Int. J. Electrochem. Sci. 9, 4747–4760. https://doi.org/10.1016/S1452-3981(23)08129-4.

Abdelhadi, R.A., Ahmed, Z.E., Abouzeid, A.M., 2023. Synthesis, spectroscopic analysis and electrochemical studies of novel organic compound based on N-alkylphthalazinone chemistry as corrosion inhibitor for carbon steel in 1M HCl. Int. J. Electrochem. Sci. 18, 100121 https://doi.org/10.1016/j.ijoes.2023.100121.

Ahmed, M.H.O., Al-Amiery, A.A., Al-Majedy, Y.K., Kadhum, A.A.H., Mohamad, A.B., Gaaz, T.S., 2018. Synthesis and characterization of a novel organic corrosion inhibitor for mild steel in 1 M hydrochloric acid. Results Phys. 8, 728–733. https://doi.org/10.1016/j.rinp.2017.12.039.

Al Otaibi, N., Hammud, H.H., 2021. Corrosion inhibition using harmal leaf extract as an eco-friendly corrosion inhibitor. Molecules 26, 7024. https://doi.org/10.3390/molecules26227024.

Al-Amiery, A.A., Ahmed, M.H.O., Abdullah, T.A., Gaaz, T.S., Kadhum, A.A.H., 2018. Electrochemical studies of novel corrosion inhibitor for mild steel in 1 M hydrochloric acid. Results Phys. 9, 978–981. https://doi.org/10.1016/j.rinp.2018.04.004.

Al-Amiery, A.A., Mohamad, A.B., Kadhum, A.A.H., Shaker, L.M., Isahak, W.N.R.W., Takriff, M.S., 2022. Experimental and theoretical study on the corrosion inhibition of mild steel by nonanedioic acid derivative in hydrochloric acid solution. Sci. Rep. 12, 4705. https://doi.org/10.1038/s41598-022-08146-8.

Al-Azawi, K.F., Al-Baghdadi, S.B., Mohamed, A.Z., Al-Amiery, A.A., Abed, T.K., Mohammed, S.A., Kadhum, A.A.H., Mohamad, A.B., 2016. Synthesis, inhibition effects and quantum chemical studies of a novel coumarin derivative on the corrosion of mild steel in a hydrochloric acid solution. Chem. Cent. J. 10, 23. https://doi.org/10.1186/s13065-016-0170-3.

Al, U.U.U.U., et, 2020. Computational study of anticorrosive effects of some thiazole derivatives against the corrosion of aluminium. RHAZES Green Appl. Chem. 10, 113–128. https://doi.org/10.48419/IMIST.PRSM/rhazes-v10.23814.

Al-Gaber, M.A.I., Abd El-Lateef, H.M., Khalaf, M.M., Shaaban, S., Shawky, M., Mohamed, G.G., Abdou, A., Gouda, M., Abu-Dief, A.M., 2023. Design, synthesis, spectroscopic inspection, DFT and Molecular docking study of metal chelates incorporating azo dye ligand for biological evaluation. Materials 16, 897. https://doi.org/10.3390/ma16030897.

Ali, I., Sh., A., Mahrous, Y., 2017. Corrosion inhibition of C-steel in acidic media from fruiting bodies of Melia azedarach L extract and a synergistic Ni 2+ additive. RSC Adv. 7, 23687–23698. https://doi.org/10.1039/C7RA00111H.

Amrhar, O., Lee, H.-S., Lgaz, H., Berisha, A., Ebenso, E.E., Cho, Y., 2023. Computational insights into the adsorption mechanisms of anionic dyes on the rutile TiO2 (110) surface: Combining SCC-DFT tight binding with quantum chemical and molecular dynamics simulations. J. Mol. Liq. 377, 121554 https://doi.org/10.1016/j.molliq.2023.121554.

Anh, H.T., Vu, N.S.H., Huyen, L.T., Tran, N.Q., Thu, H.T., Bach, L.X., Trinh, Q.T., Prabhakar Vattikuti, S.V., Nam, N.D., 2020. Ficus racemosa leaf extract for inhibiting steel corrosion in a hydrochloric acid medium. Alex. Eng. J. 59, 4449–4462. https://doi.org/10.1016/j.aej.2020.07.051.

Arrousse, N., Fernine, Y., Al-Zaqri, N., Boshaala, A., Ech-chihbi, E., Salim, R., Hajjaji, F. E., Alami, A., Ebn Touhami, M., Taleb, M., 2022. Thiophene derivatives as corrosion inhibitors for 2024–T3 aluminum alloy in hydrochloric acid medium. RSC Adv. 12, 10321–10335. https://doi.org/10.1039/D2RA00185C.

Assad, H., Kumar, A., 2021. Understanding functional group effect on corrosion inhibition efficiency of selected organic compounds. J. Mol. Liq. 344, 117755 https://doi.org/10.1016/j.molliq.2021.117755.

Ating, E.I., Umoren, S.A., Udousoro, I.I., Ebenso, E.E., Udoh, A.P., 2010. Leaves extract of Ananas sativum as green corrosion inhibitor for aluminium in hydrochloric acid solutions. Green Chem. Lett. Rev. 3, 61–68. https://doi.org/10.1080/17518250903505253.

Azzam, E.M.S., Gad, E.A.M., Al-Fahemi, J.H., 2020. Experimental and theoretical study on triazole derivatives as chelating agents to remove Fe++ Ions from wastewater in oil field. J. Heterocycl. Chem. 57, 2586–2596. https://doi.org/10.1002/jhet.3976.

Bedair, M.A., Elaryian, H.M., Gad, E.S., Alshareef, M., Bedair, A.H., Aboushahba, R.M., Fouda, A.E.-A.S., n.d. Insights into the adsorption and corrosion inhibition properties of newly synthesized diazinyl derivatives for mild steel in hydrochloric acid: synthesis, electrochemical, SRB biological resistivity and quantum chemical calculations. RSC Adv. 13, 478–498. https://doi.org/10.1039/d2ra06574f.

Belafhaili, A., El Hawary, M., Bellaouchou, A., Guenbour, A., Warad, I., Zarrouk, A., 2023. Omeprazoles inhibitive activity on the corrosion of the Al alloy in 0.5 M H2SO4 solution. Anal. Bioanal. Electrochem. 15. https://doi.org/10.22034/abec.2023.702330.

Belal, K., El-Askalany, A.H., Ghaith, E.A., Molouk, F.S., A.,, 2023. Novel synthesized triazole derivatives as effective corrosion inhibitors for carbon steel in 1M HCl solution: experimental and computational studies. Sci. Rep. 13, 22180. https://doi.org/10.1038/s41598-023-49468-5.

Boudalia, M., Fernández-Domene, R.M., Guo, L., Echihi, S., Belghiti, M.E., Zarrouk, A., Bellaouchou, A., Guenbour, A., García-Antón, J., 2023. Experimental and theoretical tests on the corrosion protection of mild steel in hydrochloric acid environment by the use of pyrazole derivative. Materials 16, 678. https://doi.org/10.3390/ma16020678.

Boukerche, S., Ferkous, H., Delimi, A., Sedik, A., Djedouani, A., Otmane Rachedi, K., Bouchoukh, H., Berredjem, M., Zahzouh, M., Himour, A., Bellucci, S., Alam, M., Benguerba, Y., 2023. Anti-corrosion performance of dehydroacetic acid thiosemicarbazone on XC38 carbon steel in an acidic medium. Arab. J. Chem. 16, 105061 https://doi.org/10.1016/j.arabjc.2023.105061.

Boumya, W., Khnifira, M., Machrouhi, A., Abdennouri, M., Sadiq, M., Achak, M., Serdaroğlu, G., Kaya, S., Şimşek, S., Barka, N., 2021. Adsorption of eriochrome black t on the chitin surface: experimental study, DFT calculations and molecular dynamics simulation. J. Mol. Liq. 331, 115706 https://doi.org/10.1016/j.molliq.2021.115706.

Cao, Y., Malekshah, R.E., Heidari, Z., Pelalak, R., Marjani, A., Shirazian, S., 2021. Molecular dynamic simulations and quantum chemical calculations of adsorption process using amino-functionalized silica. J. Mol. Liq. 330, 115544 https://doi.org/10.1016/j.molliq.2021.115544.

Chadili, M., Rguiti, M.M., El Ibrahimi, B., Oukhrib, R., Jmiai, A., Beelkhaouda, M., Bammou, L., Hilali, M., Bazzi, L., 2021a. Corrosion inhibition of 3003 aluminum alloy in molar hydrochloric acid solution by olive oil mill liquid by-product. Int. J. Corros. 2021, e6662395.

Chadili, M., Rguiti, M.M., El Ibrahimi, B., Oukhrib, R., Jmiai, A., Beelkhaouda, M., Bammou, L., Hilali, M., Bazzi, L., 2021b. Corrosion inhibition of 3003 aluminum alloy in molar hydrochloric acid solution by olive oil mill liquid by-product. Int. J. Corros. 2021, 1–13. https://doi.org/10.1155/2021/6662395.

Chakravarthy, M.P., Mohana, K.N., Pradeep Kumar, C.B., 2014. Corrosion inhibition effect and adsorption behaviour of nicotinamide derivatives on mild steel in hydrochloric acid solution. Int. J. Ind. Chem. 5, 19. https://doi.org/10.1007/s40090-014-0019-3.

Chen, X., Chen, Y., Cui, J., Li, Y., Liang, Y., Cao, G., 2021. Molecular dynamics simulation and DFT calculation of "green" scale and corrosion inhibitor. Comput. Mater. Sci. 188, 110229 https://doi.org/10.1016/j.commatsci.2020.110229.
Chung, N.T., So, Y.-S., Kim, W.-C., Kim, J.-G., 2021. Evaluation of the influence of the combination of pH, chloride, and sulfate on the corrosion behavior of pipeline steel in soil using response surface methodology. Materials 14, 6596. https://doi.org/10.3390/ma14216596.
Corrosion Inhibitive Potentials of some 2H-1-benzopyran-2-one Derivatives- DFT Calculations, 2021. . Biointerface Res. Appl. Chem. 11, 13968–13981. https://doi.org/10.33263/BRIAC116.1396813981.
Dagdag, O., Berisha, A., Safi, Z., Hamed, O., Jodeh, S., Verma, C., Ebenso, E.E., El Harfi, A., 2020. DGEBA-polyaminoamide as effective anti-corrosive material for 15CDV6 steel in NaCl medium: computational and experimental studies. J. Appl. Polym. Sci. 137, 48402. https://doi.org/10.1002/app.48402.
Daoudi, W., El Aatiaoui, A., Falil, N., Azzouzi, M., Berisha, A., Olasunkanmi, L.O., Dagdag, O., Ebenso, E.E., Koudad, M., Aouinti, A., Loutou, M., Oussaid, A., 2022. Essential oil of Dysphania ambrosioides as a green corrosion inhibitor for mild steel in HCl solution. J. Mol. Liq. 363, 119839 https://doi.org/10.1016/j.molliq.2022.119839.
Deepa, P., Padmalatha, R., 2017. Corrosion behaviour of 6063 aluminium alloy in acidic and in alkaline media. Arab. J. Chem. 10, S2234–S2244. https://doi.org/10.1016/j.arabjc.2013.07.059.
Deyab, M.A., Guibal, E., 2020. Enhancement of corrosion resistance of the cooling systems in desalination plants by green inhibitor. Sci. Rep. 10, 4812. https://doi.org/10.1038/s41598-020-61810-9.
Ebenso, E.E., Verma, C., Olasunkanmi, L.O., Akpan, E.D., Verma, D.K., Lgaz, H., Guo, L., Kaya, S., Quraishi, M.A., 2021. Molecular modelling of compounds used for corrosion inhibition studies: a review. Phys. Chem. Chem. Phys. 23, 19987–20027. https://doi.org/10.1039/d1cp00244a.
El Mazyani, A., Chafi, M., Essahli, M., 2021. Assessment of AA5005 aluminum alloy corrosion resistance by Direct Blue 15 inhibitor in sodium chloride medium. Mater. Today Proc. 37, 3882–3888. https://doi.org/10.1016/j.matpr.2020.08.473.
El-Katori, E.E., El-Saeed, R.A., Abdou, M.M., 2022. Anti-corrosion and anti-microbial evaluation of novel water-soluble bis azo pyrazole derivative for carbon steel pipelines in petroleum industries by experimental and theoretical studies. Arab. J. Chem. 15, 104373 https://doi.org/10.1016/j.arabjc.2022.104373.
El-Sayed, A.-R., El-Hendawy, M.M., El-Mahdy, M.S., Hassan, F.S.M., Mohamed, A.E., 2023. The inhibitive action of 2-mercaptobenzothiazole on the porosity of corrosion film formed on aluminum and aluminum–titanium alloys in hydrochloric acid solution. Sci. Rep. 13, 4812. https://doi.org/10.1038/s41598-023-31795-2.
Faustin, M., Maciuk, A., Salvin, P., Roos, C., Lebrini, M., 2015. Corrosion inhibition of C38 steel by alkaloids extract of Geissospermum laeve in 1M hydrochloric acid: electrochemical and phytochemical studies. Corros. Sci. 92, 287–300. https://doi.org/10.1016/j.corsci.2014.12.005.
Feng, L., Yang, H., Cui, X., Chen, D., Li, G., 2018. Experimental and theoretical investigation on corrosion inhibitive properties of steel rebar by a newly designed environmentally friendly inhibitor formula. RSC Adv. 8, 6507–6518. https://doi.org/10.1039/C7RA13045G.
Fiori-Bimbi, M.V., Alvarez, P.E., Vaca, H., Gervasi, C.A., 2015. Corrosion inhibition of mild steel in HCL solution by pectin. Corros. Sci. 92, 192–199. https://doi.org/10.1016/j.corsci.2014.12.002.
Fouda, A.S., Diab, M., El-Bindary, A., Bakr, A., 2012. Inhibition of corrosion of carbon steel in 0.5 M HCl solutions by some pyridoprymidine derivatives. Sci. J. Damietta Fac. Sci. 1, 19–31. https://doi.org/10.21608/sjdfs.2012.194252.
Fouda, A.S., Shalabi, K., Elewady, G.Y., Merayyed, H.F., 2014. Chalcone derivatives as corrosion inhibitors for carbon steel in 1 M HCl solutions. Int. J. Electrochem. Sci. 9, 7038–7058. https://doi.org/10.1016/S1452-3981(23)10950-3.
Fouda, A.S., El-Wahab, S.M.A., Attia, M.S., Youssef, A.O., Elmoher, H.O., 2015. Chemical and electrochemical studies of para-hydroazo-pyrazolone derivatives as corrosion inhibitors for mild steel in hydrochloric acid solutions. Int. J. Electrochem. Sci. 10, 7866–7892. https://doi.org/10.1016/S1452-3981(23)17396-2.
Fouda, A.S., Megahed, H.E., Fouad, N., Elbahrawi, N.M., 2016. Corrosion inhibition of carbon steel in 1 M hydrochloric acid solution by aqueous extract of thevetia peruviana. J. Bio- Tribo-Corros. 2, 16. https://doi.org/10.1007/s40735-016-0046-z.
Fouda, A.S., Ismail, M.A., Khaled, M.A., El-Hossiany, A.A., 2022. Experimental and computational chemical studies on the corrosion inhibition of new pyrimidinone derivatives for copper in nitric acid. Sci. Rep. 12, 1–19. https://doi.org/10.1038/s41598-022-20306-4.
Gaber, G.A., Mohamed, L.Z., Tash, M.M., 2020. Experimental correlation using ANOVA and DOE studies on corrosion behavior of Fe and Ni-based alloy under different media. Mater. Res. Express 7, 036521. https://doi.org/10.1088/2053-1591/ab7e6d.
Ganjoo, R., Sharma, S., Thakur, A., Assad, H., Kumar Sharma, P., Dagdag, O., Berisha, A., Seydou, M., Ebenso, E.E., Kumar, A., 2022a. Experimental and theoretical study of Sodium Cocoyl Glycinate as corrosion inhibitor for mild steel in hydrochloric acid medium. J. Mol. Liq. 364, 119988 https://doi.org/10.1016/j.molliq.2022.119988.
Ganjoo, R., Verma, C., Kumar, A., Quraishi, M.A., 2022b. Colloidal and interface aqueous chemistry of dyes: past, present and future scenarios in corrosion mitigation. Adv. Colloid Interface Sci. 102832.
Guo, L., Zhu, M., Chang, J., Thomas, R., Zhang, R., Wang, P., Zheng, X., Lin, Y., Marzouki, R., 2021. Corrosion inhibition of N80 steel by newly synthesized imidazoline based ionic liquid in 15% HCl medium: experimental and theoretical investigations. Int. J. Electrochem. Sci. 16, 211139. https://doi.org/10.20964/2021.11.15.
Gupta, S.K., Mehta, R.K., Yadav, M., Dagdag, O., Mehmeti, V., Berisha, A., Ebenso, E.E., 2023. Diazenyl derivatives as efficient corrosion inhibitors for mild steel in HCl medium: gravimetric, electrochemical and computational approach. J. Mol. Liq. 382, 121976 https://doi.org/10.1016/j.molliq.2023.121976.
Hadisaputra, S., Purwoko, A.A., Hakim, A., Prasetyo, N., Hamdiani, S., 2022. Corrosion inhibition properties of phenyl phthalimide derivatives against carbon steel in the acidic medium: DFT, MP2, and Monte carlo simulation studies. ACS Omega 7, 33054–33066. https://doi.org/10.1021/acsomega.2c03091.
Halambek, J., Berković, K., 2012. Inhibitive action of anethum graveolens l. Oil on aluminium corrosion in acidic media. Int. J. Electrochem. Sci. 7 https://doi.org/10.1016/S1452-3981(23)17999-5.
Halambek, J., Jukić, M., Berković, K., Vorkapić-Furač, J., 2012. Investigation of novel heterocyclic compounds as inhibitors of Al-3Mg alloy corrosion in hydrochloric acid solutions. Int. J. Electrochem. Sci. 7, 1580–1601. https://doi.org/10.1016/S1452-3981(23)13437-7.
Haldhar, R., Prasad, D., Nguyen, L.T.D., Kaya, S., Bahadur, I., Dagdag, O., Kim, S.-C., 2021. Corrosion inhibition, surface adsorption and computational studies of Swertia chirata extract: a sustainable and green approach. Mater. Chem. Phys. 267, 124613 https://doi.org/10.1016/j.matchemphys.2021.124613.
Haris, N.I.N., Sobri, S., Yusof, Y.A., Kassim, N.K., 2021. An overview of molecular dynamic simulation for corrosion inhibition of ferrous metals. Metals 11, 46. https://doi.org/10.3390/met11010046.
Harvey, T.J., Walsh, F.C., Nahlé, A.H., 2018. A review of inhibitors for the corrosion of transition metals in aqueous acids. J. Mol. Liq. 266, 160–175. https://doi.org/10.1016/j.molliq.2018.06.014.
Hussin, M.H., Rahim, A.A., Mohamad Ibrahim, M.N., Brosse, N., 2016. The capability of ultrafiltrated alkaline and organosolv oil palm (Elaeis guineensis) fronds lignin as green corrosion inhibitor for mild steel in 0.5 M HCl solution. Measurement 78, 90–103. https://doi.org/10.1016/j.measurement.2015.10.007.
Ikeuba, A.I., Ntibi, J.E., Okafor, P.C., Ita, B.I., Agobi, A.U., Asogwa, F.C., Omang, B.J., Eno, E.A., Loius, H., Adalikwu, S.A., Abiola, B.A., Abeng, F.E., Abang, N.A., 2023. Kinetic and thermodynamic evaluation of azithromycin as a green corrosion inhibitor during acid cleaning process of mild steel using an experimental and theoretical approach. Results Chem. 5, 100909 https://doi.org/10.1016/j.rechem.2023.100909.
Iorhuna, F., Muhammad, A., Ayuba, M., 2023. Quinazoline derivatives as corrosion inhibitors on aluminium metal surface: a theoretical study. Adv. J. Chem.-Sect. A 6. https://doi.org/10.22034/ajca.2023.370123.1347.
Ismail, M.A., Shaban, M.M., Abdel-Latif, E., Abdelhamed, F.H., Migahed, M.A., El-Haddad, M.N., Abousalem, A.S., 2022. Novel cationic aryl bithiophene/terthiophene derivatives as corrosion inhibitors by chemical, electrochemical and surface investigations. Sci. Rep. 12, 3192. https://doi.org/10.1038/s41598-022-06863-8.
K, U., V, R., S, R., 2016. The effect of inhibitor on the corrosion of aluminium in acidic solutions. SOJ Mater. Sci. Eng. 4. https://doi.org/10.15226/sojmse.2016.00140.
Kellal, R., Benmessaoud Left, D., Safi, Z.S., Wazzan, N., Al-Qurashi, O.S., Zertoubi, M., 2023a. A new approach for the evaluation of liquid waste generated from plant extraction process for the corrosion mitigation of carbon steel in acidic medium: case of Chrysanthemum Coronarium stems. J. Ind. Eng. Chem. 125, 370–389. https://doi.org/10.1016/j.jiec.2023.05.046.
Kellal, R., Left, D.B., Azzi, M., Zertoubi, M., 2023b. Insight on the corrosion inhibition performance of Glebionis coronaria plant extract in various acidic mediums. J. Appl. Electrochem. 53, 811–832. https://doi.org/10.1007/s10800-022-01813-8.
Kim, Y., Choi, J., 2021. Oxide growth characteristics on Al (100), (110), and (111) surfaces: a chemo-mechanical evaluation. Mater. Today Commun. 26, 102006 https://doi.org/10.1016/j.mtcomm.2020.102006.
Klamt, A., 2018. The COSMO and COSMO-RS solvation models. Wires Comput. Mol. Sci. 8, e1338.
Kumar, T., Vishwanatham, S., Udayabhanu, G., 2004. Synergistic effects of formaldehyde and alcoholic extract of plant leaves for protection of N80 steel in 15%HCl. Corros. Eng. Sci. Technol. 39, 327–332. https://doi.org/10.1179/174327804X13181.
Lebrini, M., Robert, F., Roos, C., 2013. Adsorption properties and inhibition of C38 steel corrosion in hydrochloric solution by some indole derivates: temperature effect, activation energies, and thermodynamics of adsorption. Int. J. Corros. 2013, 1–13. https://doi.org/10.1155/2013/139798.
Lee, W.-J., Pyun, S.-I., 1999. Effects of hydroxide ion addition on anodic dissolution of pure aluminium in chloride ion-containing solution. Electrochim. Acta 44, 4041–4049. https://doi.org/10.1016/S0013-4686(99)00164-4.
Lgaz, H., Chaouiki, A., Al-Hadeethi, M.R., Salghi, R., Lee, H.-S., 2021. Computational methods of corrosion monitoring. In: Organic Corrosion Inhibitors. John Wiley & Sons Ltd, pp. 39–57. https://doi.org/10.1002/9781119794516.ch3.
Li, D.G., Wang, J.D., Chen, D.R., Liang, P., 2015. Influence of molybdenum on tribo-corrosion behavior of 316L stainless steel in artificial saliva. J. Bio- Tribo-Corros. 1, 14. https://doi.org/10.1007/s40735-015-0014-z.
Li, X.-L., Xie, B., Lai, C., Feng, J.-S., Liu, X.-Q., Chen, L., Yang, Y.-G., Ji, R.-W., He, J.-Y., Li, W., Liu, M.-N., 2022. Adsorption and corrosion inhibition performance of two planar rigid pyridinecarboxaldehyde-based double Schiff bases for mild steel in HCl solution: experimental and computational investigations. J. Mol. Liq. 355, 118926 https://doi.org/10.1016/j.molliq.2022.118926.
Lim, M.C.G., Zhong, Z.W., 2009. Molecular dynamics analyses of an Al(110)<math><mstyle mathvariant="normal" is="true"><mi is="true">Al</mi></mstyle><mrow is="true"><mo is="true">(</mo><mn is="true">110</mn><mo is="true">)</mo></mrow></math> surface. Phys. Stat. Mech. Its Appl. 388, 4083–4090. https://doi.org/10.1016/j.physa.2009.06.043.
Lin, B., Shao, J., Xu, Y., Lai, Y., Zhao, Z., 2021. Adsorption and corrosion of renewable inhibitor of Pomelo peel extract for mild steel in phosphoric acid solution. Arab. J. Chem. 14, 103114 https://doi.org/10.1016/j.arabjc.2021.103114.
Madkour, L.H., Kaya, S., Kaya, C., Guo, L., 2016. Quantum chemical calculations, molecular dynamics simulation and experimental studies of using some azo dyes as

corrosion inhibitors for iron. Part 1: Mono-azo dye derivatives. J. Taiwan Inst. Chem. Eng. 68, 461–480. https://doi.org/10.1016/j.jtice.2016.09.015.
Mehmeti, V., Podvorica, F.I., 2018. Experimental and theoretical studies on corrosion inhibition of niobium and tantalum surfaces by carboxylated graphene oxide. Materials 11, 893. https://doi.org/10.3390/ma11060893.
Melian, R., Radi, M., Hachimi, F.E., Galai, M., Ouakki, M., El Assiri, E.H., Guo, L., Dkhirche, N., Touhami, M.E., 2023. Detailedexperimental and computational explorations of two heterocyclic compounds as corrosion inhibitors for aluminum alloy 2024–T3 in 3.5% NaCl: electrochemical/surface studies, DFT/MD modeling. Inorg. Chem. Commun. 152, 110679 https://doi.org/10.1016/j.inoche.2023.110679.
Migahed, A.M., Zaki, G.E., Shaban, M., 2016. Corrosion control in the tubing steel of oil wells during matrix acidizing operations. RSC Adv. 6, 71384–71396. https://doi.org/10.1039/C6RA12835A.
Mohsenifar, F., Jafari, H., Sayin, K., 2016. Investigation of thermodynamic parameters for steel corrosion in acidic solution in the presence of N, N′-bis (phloroacetophenone)-1,2 propanediamine. J. Bio- Tribo-Corros. 2, 1. https://doi.org/10.1007/s40735-015-0031-y.
Nyijime, T.A., Chahul, H.F., Ayuba, A.M., Iorhuna, F., 2023. Theoretical investigations on thiadiazole derivatives as corrosion inhibitors on mild steel. Adv. J. Chem. Sect. A 6, 141–154. https://doi.org/10.22034/ajca.2023.383496.1352.
Obot, I.B., Gasem, Z.M., 2014. Theoretical evaluation of corrosion inhibition performance of some pyrazine derivatives. Corros. Sci. 83, 359–366. https://doi.org/10.1016/j.corsci.2014.03.008.
Oki, M., Oki, K., Otaigbe, J., Otikor, S., 2013. Corrosion inhibition of aluminium in HCl by amine modified epoxy resin. J. Mater. 2013, 1–5. https://doi.org/10.1155/2013/479728.
Oladoye, P.O., Bamigboye, M.O., Ogunbiyi, O.D., Akano, M.T., 2022. Toxicity and decontamination strategies of Congo red dye. Groundw. Sustain. Dev. 19, 100844 https://doi.org/10.1016/j.gsd.2022.100844.
Padash, R., Jafari, A.H., Jamalizadeh, E., 2018. Experimental and theoretical study of aluminium corrosion in NaOH, NaCl and HCl solutions. Anti-Corros. Methods Mater. 65, 350–360. https://doi.org/10.1108/ACMM-04-2017-1785.
Padash, R., Sajadi, G.S., Jafari, A.H., Jamalizadeh, E., Rad, A.S., 2020. Corrosion control of aluminum in the solutions of NaCl, HCl and NaOH using 2,6-dimethylpyridine inhibitor: experimental and DFT insights. Mater. Chem. Phys. 244, 122681 https://doi.org/10.1016/j.matchemphys.2020.122681.
Pareek, S., Jain, D., Hussain, S., Biswas, A., Shrivastava, R., Parida, S.K., Kisan, H.K., Lgaz, H., Chung, I.-M., Behera, D., 2019. A new insight into corrosion inhibition mechanism of copper in aerated 3.5 wt.% NaCl solution by eco-friendly imidazopyrimidine dye: experimental and theoretical approach. Chem. Eng. J. 358, 725–742. https://doi.org/10.1016/j.cej.2018.08.079.
Parlak, A.E., Omar, R.A., Koparir, P., Salih, M.I., 2022. Experimental, DFT and theoretical corrosion study for 4-(((4-ethyl-5-(thiophen-2-yl)-4H-1,2,4-triazole-3-yl) thio)methyl)-7,8-dimethyl-2H-chromen-2-one. Arab. J. Chem. 15, 104088 https://doi.org/10.1016/j.arabjc.2022.104088.
Paşka, O., Ianoş, R., Păcurariu, C., Brădeanu, A., 2014. Magnetic nanopowder as effective adsorbent for the removal of Congo Red from aqueous solution. Water Sci. Technol. J. Int. Assoc. Water Pollut. Res. 69, 1234–1240. https://doi.org/10.2166/wst.2013.827.
Pucci, R., Angilella, G.G.N., 2022. Density functional theory, chemical reactivity, and the Fukui functions. Found. Chem. 24, 59–71. https://doi.org/10.1007/s10698-022-09416-z.
Qiang, Y., Zhang, S., Tan, B., Chen, S., 2018. Evaluation of Ginkgo leaf extract as an eco-friendly corrosion inhibitor of X70 steel in HCl solution. Corros. Sci. 133, 6–16. https://doi.org/10.1016/j.corsci.2018.01.008.
Quebbou, Z., Chafi, M., Omari, L.E.H., 2021. Corrosion resistance of 5005 aluminum alloy by anodizing treatment in a mixture of phosphoric and boric acids. Mater. Today Proc. 37, 3854–3859. https://doi.org/10.1016/j.matpr.2020.08.406.
Raghavendra, N., Ishwara Bhat, J., 2018. Benevolent behavior of arecanut husk extracts as potential corrosion inhibitor for aluminum in both 0.5 M HCl and 0.1 M NaOH Environments. J. Bio- Tribo-Corros. 4, 44. https://doi.org/10.1007/s40735-018-0159-7.
Raviprabha, K., Bhat, R.S., Bhat, S.I., Nagaraj, P., Jyothi, K., 2023. Corrosion inhibition study of 6061 aluminium alloy in the presence of ethyl 5-methyl-1-(4-nitrophenyl)-1H-1,2,3-triazole-4-carboxylate (NTE) in hydrochloric acid. Heliyon 9, e16036.
Reena Kumari, P.D., Nayak, J., Nityananda Shetty, A., 2016. Corrosion behavior of 6061/Al-15 vol. pct. SiC(p) composite and the base alloy in sodium hydroxide solution. Arab. J. Chem. 9, S1144–S1154. https://doi.org/10.1016/j.arabjc.2011.12.003.
Rugmini Ammal, P., Prasad, A.R., Joseph, A., 2018. Comparative studies on the electrochemical and physicochemical behaviour of three different benzimidazole motifs as corrosion inhibitor for mild steel in hydrochloric acid. Egypt. J. Pet. 27, 1067–1076. https://doi.org/10.1016/j.ejpe.2018.03.006.
Salman, T., 2020. Inhibition studies of aluminium alloy (2024) corrosion in acid hydrochloride solution using an expired phenylphrine drug. Egypt. J. Chem. https://doi.org/10.21608/ejchem.2020.19583.2222.
Sanni, O., Iwarere, S.A., Daramola, M.O., 2022. Evaluation of corrosion inhibition of essential oil-based inhibitors on aluminum alloys. ACS Omega 7, 40740–40749. https://doi.org/10.1021/acsomega.2c00540.
Saraçoğlu, M., Elusta, M.I.A., Kaya, S., Kaya, C., Kandemirli, F., 2018. Quantum chemical studies on the corrosion inhibition of Fe78B13Si9 glassy alloy in Na2SO4 solution of some thiosemicarbazone derivatives. Int. J. Electrochem. Sci. 13, 8241–8259. https://doi.org/10.20964/2018.08.74.
Shainy, K.M., Rugmini Ammal, P., Unni, K.N., Benjamin, S., Joseph, A., 2016. Surface interaction and corrosion inhibition of mild steel in hydrochloric acid using pyoverdine, an eco-friendly bio-molecule. J. Bio- Tribo-Corros. 2, 20. https://doi.org/10.1007/s40735-016-0050-3.
Shivakumar, S.S., Mohana, K.N., 2013. Corrosion behavior and adsorption thermodynamics of some schiff bases on mild steel corrosion in industrial water medium. Int. J. Corros. 2013, 1–13. https://doi.org/10.1155/2013/543204.
Soltani, N., Tavakkoli, N., Ghasemi, M., 2016. Corrosion inhibition of low carbon steel by extract as green corrosion inhibitor in hydrochloric acid solution. Int. J. Electrochem. Sci. 11, 8827–8847. https://doi.org/10.20964/2016.10.22.
Souza, L., Pereira, E., Matlakhova, L., Nicolin, V.A.F., Monteiro, S.N., De Azevedo, A.R. G., 2023. Ionic liquids as corrosion inhibitors for carbon steel protection in hydrochloric acid solution: a first review. J. Mater. Res. Technol. 22, 2186–2205. https://doi.org/10.1016/j.jmrt.2022.12.066.
Tezcan, F., Yerlikaya, G., Mahmood, A., Kardaş, G., 2018. A novel thiophene Schiff base as an efficient corrosion inhibitor for mild steel in 1.0 M HCl: Electrochemical and quantum chemical studies. J. Mol. Liq. 269, 398–406. https://doi.org/10.1016/j.molliq.2018.08.025.
Thoume, A., Benmessaoud Left, D., Elmakssoudi, A., Benhiba, F., Zarrouk, A., Benzbiria, N., Warad, I., Dakir, M., Azzi, M., Zertoubi, M., 2021. Chalcone oxime derivatives as new inhibitors corrosion of carbon steel in 1 M HCl solution. J. Mol. Liq. 337, 116398 https://doi.org/10.1016/j.molliq.2021.116398.
Toukal, L., Keraghel, S., Benghanem, F., Ourari, A., 2018. Electrochemical, thermodynamic and quantum chemical studies of synthesized benzimidazole derivative as an eco-friendly corrosion inhibitor for XC52 steel in hydrochloric acid. Int. J. Electrochem. Sci. 13, 951–974. https://doi.org/10.20964/2018.01.43.
Umar, B.A., Uzairu, A., 2019. In-silico approach to understand the inhibition of corrosion by some potent triazole derivatives of pyrimidine for steel. SN Appl. Sci. 1, 1413. https://doi.org/10.1007/s42452-019-1451-y.
Verma, C., Lgaz, H., Verma, D.K., Ebenso, E.E., Bahadur, I., Quraishi, M.A., 2018. Molecular dynamics and Monte Carlo simulations as powerful tools for study of interfacial adsorption behavior of corrosion inhibitors in aqueous phase: a review. J. Mol. Liq. 260, 99–120. https://doi.org/10.1016/j.molliq.2018.03.045.
Verma, C., Hussain, C.M., Quraishi, M.A., Alfantazi, A., 2023. Green surfactants for corrosion control: design, performance and applications. Adv. Colloid Interface Sci. 311, 102822 https://doi.org/10.1016/j.cis.2022.102822.
Wang, Z., Zou, Y., Xiao, K., Fan, Y., Wang, S., 2022. Corrosion behavior of aluminum in some short-chain carboxylic acid solutions as a simulant for cooling water in HVDC transmission. Int. J. Electrochem. Sci. 17, 221254. https://doi.org/10.20964/2022.12.54.
Yoo, H., Lee, C., Oh, K., Choi, J., 2016. Effects of metal anion complexes in electrolyte on the properties of anodic oxide films on ADC12 Al alloy. J. Korean Inst. Surf. Eng. 49, 130–134. https://doi.org/10.5695/JKISE.2016.49.2.130.
Zarrouk, A., Hammouti, B., Zarrok, H., Al-Deyab, S.S., Messali, M., 2011. Temperature effect, activation energies and thermodynamic adsorption studies of L-Cysteine methyl ester hydrochloride as copper corrosion inhibitor in nitric acid 2m. Int. J. Electrochem. Sci. 6, 6261–6274. https://doi.org/10.1016/S1452-3981(23)19679-9.
Zeinali Nikoo, S., Shockravi, A., Mokarami Ghartavol, H., Halimehjani, A.Z., Ostadrahimi, M., Mirhosseini, S.M., Behzadi, H., Ghorbani, M., 2020. A study of glycine-based dithiocarbamates as effective corrosion inhibitors for cold rolled carbon steel in HCl solutions. Surf. Interfaces 21, 100751. https://doi.org/10.1016/j.surfin.2020.100751.
Zeng, J.-P., Wang, F.-H., Gong, X.-D., 2013. Molecular dynamics simulation of the interaction between polyaspartic acid and calcium carbonate. Mol. Simul. 39, 169–175. https://doi.org/10.1080/08927022.2012.709632.
Zhao, T., Munis, A., Rehman, A.U., Zheng, M., 2020. Corrosion behavior of aluminum in molten hydrated salt phase change materials for thermal energy storage. Mater. Res. Express 7, 015529. https://doi.org/10.1088/2053-1591/ab6c24.
Zhao, Q., Tang, T., Dang, P., Zhang, Z., Wang, F., 2017. The corrosion inhibition effect of triazinedithiol inhibitors for aluminum alloy in a 1 M HCl solution. Metals 7, 44. https://doi.org/10.3390/met7020044.